Technische Universität München
TUM School of Medicine and Health

TIM

Characterization of the radioresponse of different pancreatic cancer patient-derived organoids

Christopher Keßler

Vollständiger Abdruck der von der TUM School of Medicine and Health der Technischen

Universität München zur Erlangung eines

Doktors der Medizinischen Wissenschaft (Dr. med. sci.)

genehmigten Dissertation.

Vorsitz: apl. Prof. Dr. Klaus-Peter Janssen

Prüfende der Dissertation:

1. Prof. Dr. Stephanie E. Combs

2. Prof. Dr. Maximilian Reichert

Die Dissertation wurde am 09.08.2023 bei der Technischen Universität München

eingereicht und durch die TUM School of Medicine and Health am 07.02.2024 angenommen.

Table of contents

List of figures

List of tables

Abbreviations

A	Ampere
AUC	Area under the curve
CA 19-9	Carbohydrate antigen 19-9
CDKN2A	Cyclin-dependent kinase inhibitor 2a
CI	Confidence interval
CSC	Cancer stem cells
CRS	Cell recovery solution
CT	Computed tomography
D_{50}	Half maximal inhibitory dose
DEG	Differentially expressed genes
DMEM	Dulbecco's Modified Eagle's Medium
DNA	Deoxyribonucleic acid
DPBS	Dulbecco's Phosphate Buffered Saline
DSB	Double strand break
ECM	Extracellular matrix
FPC	Familial pancreatic cancer
GDP	Guanosine diphosphate
GSEA	Gene set enrichment analysis
GES	Gene expression signatures
GTP	Guanosine triphosphate
Gy	Gray (absorbed dose of ionizing radiation)
HE	Hematoxylin and eosin
HIF	Hypoxia-inducible factor
H	Hour(s)
HR	Hazard ratio
IHC	Immunohistochemistry
IPMN	Intraductal papillary mucinous neoplasm
ITPN	Intratubular papillary neoplasm
KRAS	Kirsten rat sarcoma oncogene

MCN	Mucinous cystic neoplasm
Min	Minutes
MRI	Magnetic resonance imaging
OS	Overall survival
OXPHOS	Oxidative phosphorylation
PanIN	Pancreatic intraepithelial neoplasm
PC	Pancreatic cancer
PDAC	Pancreatic ductal adenocarcinoma
PDO	Patient-derived organoid
PET	Positron emission tomography
PFS	Progression free survival
PSC	Pancreatic stellate cells
RNA	Ribonucleic acid
rpm	Revolutions per minute
RCT	Radiochemotherapy
RT	Radiotherapy
RTOG	Radiation Therapy Oncology Group
SD	Standard deviation
SPARC	Secreted protein acidic and rich in cysteine
TME	Tumor microenvironment
TP53	Tumor protein p53
TUM	Technical University of Munich
V	Volt

1. Introduction

1.1. Pancreatic ductal adenocarcinoma

1.1.1. Epidemiology

The pancreatic ductal adenocarcinoma (PDAC) is with a share of 90% by far the most frequent of the pancreatic neoplasms (Stewart & Wild, 2014, p. 413). Therefore, the term pancreatic cancer (PC) is conterminously used for PDAC in this thesis.

In 2018 PC was ranked 7th (19 067 cases per year) in Germany and 11th (50 846 cases per year) in the U.S. in a comparison of the most common cancer sites by incidence, with hardly any difference between sexes (Ferlay et al., 2018). The mortality rates nearly equal the incidence rates, ranking PC on place two in Germany in deaths due to cancer in 2021 (Destatis, 2022). Worldwide PC is only the 7th (432 000 deceased) leading cause of cancer-related deaths, however having a three-to four-fold greater incidence in countries with higher rankings in the Human Development Index (Bray et al., 2018, p. 421). In Germany the PC incidence is two- to threefold higher in comparison to 40 years ago and is expected to keep rising by 2.0% for man and 0.8% for woman every year (ZfKD-RKI, 2016, pp. 61-63).

The majority of the patients are aged between 65-84 years. Due to the aggressiveness and the late onset of the symptoms, in 85-90% of the cases the tumor is already inoperable or has developed metastases (Kasper et al., 2016, p. 675). This leads to a mean 5-year survival rate of less than 10% (Park, Chawla, & O'Reilly, 2021).

1.1.2. Risk factors

As shown before, age is the major factor negatively affecting the risk of getting PC during a lifespan. Nevertheless, there are many other influences changing the probability for PC. Most of these known risk factors relate to unhealthy living habits.

Cigarette smoking is one of the best investigated factors. Recent studies show that current cigarette smokers averagely twofold their risk for PC, rising linearly

with the duration of smoking years. The risk levels are 20% higher for former smokers, reaching the levels of non-smokers approximately 20 years after starting the abstinence (Bosetti et al., 2012, p. 1884).

Alcohol intake at high rates (>60g/d) significantly elevates the risk for PC with a hazard ratio (HR) of 1.63 in comparison to moderate drinkers (0.1-4.9 g/d), probably due to the high production of acetaledehyde, a carcinogenic metabolic degradation product of alcohol. Interestingly, this rise in the HR is only visible in men and not in women (Naudin et al., 2018). Alcohol intake can lead to pancreatitis, which is also a known risk factor for PC. Also, smoking was thought to have a reinforcing effect on alcohol induced PC, beside its own carcinogenic impact. But Naudin et al. (2018) could show in their analysis of the "European Prospective Investigation into Cancer and Nutrition (EPIC)", that neither the alcohol induced chronic pancreatitis was the main course for PC in context with consumption of alcohol nor, that cigarette smoking had an enhancing effect on the carcinogenic potential of alcohol abuse.

High physical activity led to a risk reduction of PC between 7% to 22% in comparison with a group performing only at low levels. Reasons for this could be the reduction of obesity and diabetes (Behrens et al., 2015, p. 293). Obesity is connected to a rise of pro inflammatory substances produced in the adipose tissue. It also enhances insulin resistance, increases circulating lipids and can induce microbiome changes, all these factors can negatively affect the PC risk. Therefore, obesity is a dangerous but highly modifiable risk factor (M. Xu, Jung, Hines, Eibl, & Chen, 2018).

Some dietary patterns are suspected to raise the possibility for PC. A low and not statistically significant correlation was calculated for a high intake of red meat. For a high intake of processed meat, however, a rise in risk of 19% could be measured, likely explained by the mutagen capacity of the therein occurring n-nitrosamines (Larsson & Wolk, 2012). In general, an animal and starch rich nutrition is correlated with increased risks of PC while a vitamin- and vegetable rich diet is correlated with lower risks (Bosetti et al., 2013).

Diabetes is another well-known risk factor. People with a diabetic history initially had a twofold increased risk in comparison to a control group. The risk decreased

corresponding to the duration of the diabetes. After 20 years this risk has fallen to only 30% higher values than measured in the control group (Bosetti et al., 2014).

Chronic pancreatitis increases the PC risk by 18 times, with 5% of the chronic pancreatitis patients developing PC in their lifetime (Kirkegard, Mortensen, & Cronin-Fenton, 2017). One main reason for this highly elevated risk is the chronic inflammation of the pancreatic tissue inducing carcinogenesis by the activation of stellate cells. Also, the risk factors smoking and alcohol abuse are often simultaneously present in these patients.

5% to 10% of all PDAC cases relate to a positive family history of PC. The risks increase twofold when a first-degree relative is diagnosed with PC and threefold if this relative is younger than 60 years (McWilliams, Rabe, Olswold, De Andrade, & Petersen, 2005).

The term "Familial pancreatic cancer" (FPC) is used when at least two first-degree relatives are diagnosed with PC. In this case, often a genetic mutation occurs in the pedigree. Genes like BRCA2, CDK2A and about 12 others are likely to play a decisive role in FPC (Petersen, 2016).

1.1.3. Carcinogenesis

PDAC mainly evolves from previously existing precursors, which gradually develop higher grades of dysplasia and finally transform into cancer (Hruban, Goggins, Parsons, & Kern, 2000). The four important precancerous lesions are: Pancreatic intraepithelial neoplasm (PanIN) being the most frequent one, intraductal papillary mucinous neoplasm (IPMN), mucinous cystic neoplasm (MCN) and intratubular papillary neoplasm (ITPN). Each of these precursors holds different histopathological features and molecular hallmarks (Riva et al., 2018).

Unexpectedly, PDAC is not exclusively evolving from ductal cells, but more often through the process of transdifferentiation mature acinar cells form facultative progenitor cells for PC (Yamaguchi, Yokoyama, Kokuryo, Ebata, & Nagino, 2018). PanIN have acinar cells as an origin (Kopp et al., 2012) whereas ductal cells seem to generate IPMNs. Another source of PanINs are Dclk1+ quiescent pancreatic progenitor cells, normally functioning as a cell reservoir for pancreatic repair after injury (Westphalen et al., 2016). However, the evolution of PDAC is

not completely understood and many studies are still investigating its development in detail.

The most frequent alteration and major driver mutation in PC is the mutationally activated protooncogene KRAS, which is existent in >90% of human PDACs (Morris, Wang, & Hebrok, 2010). Wildtype KRAS transduces signals from the cell surface to downstream effectors. The most frequent mutation in the KRAS gene is a substitution in G12 or G13, which changes the molecular structure in its binding site. This prevents GTP from hydrolysis and therefore KRAS constantly activates downstream pathways, leading to higher rates of proliferation, suppression of apoptosis, remodeling of the microenvironment, evasion of the immune response and acquiring of metastatic capacities (Pylayeva-Gupta, Grabocka, & Bar-Sagi, 2011). Above that, the shaping of the multiple downstream signaling pathways of KRAS seems to vary between different tumor sub-identities (Eser, Schnieke, Schneider, & Saur, 2014). Not only the presence of a KRAS mutation, but furthermore the amplification of its gene dosage increases the tumor's aggressiveness and metastatic potential, defining the different characteristics of PC (Mueller et al., 2018).

The mutational landscape is not limited to KRAS expressing in a high heterogeneity of the tumors individual genetic aberrations (Cowley et al., 2013). Other high frequent mutations appear in the tumor suppressors CDKN2A, TP53 and SMAD4. These mutational burdens seem to accumulate in later stages of the tumor progression model from early precursors to cancer (Dunne & Hezel, 2015). Jones et al. (2008) discovered that the mutated genes are highly differing from tumor to tumor, but that most of these alterations can be assigned to one of 12 different pathways, explaining both the heterogeneity and the central similarities between PC.

Another piece of the puzzle in explaining the tumor's aggressiveness is the model of cancer stem cells (CSC). These treatment resistant cells carry inherent self-renewal capacities and own high grades of plasticity. They can generate bulk cancer cells, which show a characteristically high proliferation rate but are much more sensitive to drug treatment. This change of state is bidirectional and the bulk cancer cells in return can give rise to the resistant and slowly dividing CSCs (Valle, Martin-Hijano, Alcalá, Alonso-Nocelo, & Sainz, 2018). The CSCs

capability to survive in hostile living conditions is not fully understood at this point, but the tumor microenvironment (TME) is assumed to play the crucial role (Hamada et al., 2012).

1.1.4. Tumor microenvironment

The TME in PC can already be noticed macroscopically due to its abundant stroma, which, with a share of 85-90% of the tumor mass, by far outnumbers the neoplastic cells (Vaziri-Gohar, Zarei, Brody, & Winter, 2018). The TME mainly consists of fibroblasts, pancreatic stellate cells (PSC), which produce large quantities of extracellular matrix (ECM), immune cells, blood cells and soluble proteins (Feig et al., 2012, p. 4267). The ECM comprises hyaluronan, collagen, fibronectin and secreted protein, acidic and rich in cysteine. This combination results in a firm and swollen tissue, which compresses the blood vessels and creates a hypoxic environment (Kanat & Ertas, 2018, p. 4268). However, in early stages the TME is assumed to be protective, whereas later in the cancer progression it enhances the tumor's aggressiveness (Bynigeri et al., 2017). The main catalysator for the TME`s harmful influence on PDAC are the PSCs. Vonlaufen et al. (2008) demonstrated *in vitro* and *in vivo* experiments that co-culturing of PSCs with PDAC-cells accelerates cancer progression by increasing proliferation rates and inhibiting apoptosis. PSCs are also critical for emerging metastases. The PSCs can migrate through endothelium and generate tumor niches at non-primary sites, in which cancer cells are able to survive (Z. Xu et al., 2010). Furthermore, the PSCs aid the tumor in avoiding immune surveillance and thereby protecting the neoplastic cells from induced apoptosis. An essential mechanism for this purpose is the sequestration of CD8+ cells in the panstromal compartment (Ene-Obong et al., 2013). Another one is the PSCs expression of galactin-1, which induces T-cell apoptosis (Tang et al., 2015).

1.1.5. Tumor classification

The TNM classification system (Table 1 and Table 2) is broadly used in clinical routine and research worldwide. It is fundamental for treatment planning, evaluation and prediction of the patient's outcome (UICC, 2017, pp. 2-3).

Table 1: TNM classification of PC (UICC, 2017).

T1	**Tumor 2 cm or less in greatest dimension**
T1a	**Tumor 0.5 cm or less in greatest dimension**
T1b	**Tumor greater than 0.5 cm and less than 1 cm in greatest dimension**
T1c	**Tumor greater than 1 cm and less than 2 cm in greatest dimension**
T2	Tumor more than 2 cm but no more than 4 cm in greatest dimension
T3	Tumor more than 4 cm in greatest dimension
T4	Tumor involves coeliac axis, superior mesenteric artery and/or common hepatic artery
N0	No regional lymph node metastasis
N1	Metastases in 1 to 3 regional lymph nodes
N2	Metastases in 4 ore more regional lymph nodes
M0	No distant metastasis
M1	Distant metastasis

Table 2: UICC stages of PC (UICC, 2017).

Stage	T	N	M
0	Tis	N0	M0
IA	T1	N0	M0
IB	T2	N0	M0
IIA	T3	N0	M0
IIB	T1 - T3	N1	M0
III	T1 - T4	Any N	M0
IV	Any T	Any N	M1

1.1.6. Clinical presentation

Due to the late and unspecific onset of symptoms, 80% of the patients have already evolved a locally advanced, mostly unresectable or metastatic disease at the time of first diagnosis (Park et al., 2021). PDAC most frequently manifests with obstructive jaundice, followed by abdominal complaints, pruritus, fatigue and weight loss. Less common symptoms are epigastric pain, back pain, newly emerging diabetes mellitus and acute pancreatitis (Kasper et al., 2016).

The diagnostic cascade after suspecting PC starts with upper abdominal sonography. Followed by either multi-slice computed tomography (CT), magnetic resonance imaging (MRI) or with a higher examiner-dependent sensitivity endosonography (Deutsche Krebsgesellschaft, 2013). The serum biomarker CA 19-9 is of high importance as it can make other differential diagnoses more improbable and can help as a marker for recurrence in follow-ups (Ritts, Nagorney, Jacobsen, Talbot, & Zurawski, 1994). It can also help to predict the tumor's unresectability as it correlates with the tumor load (Forsmark, Lambiase, & Vogel, 1994).

1.1.7. Treatment

The only curative treatment for PC still is the complete resection of the tumor. Standalone radiochemotherapy (RCT) is not suitable for non-palliative approaches (Doi et al., 2008). The tumor is classified as unresectable if it has encased either the superior mesenteric artery or the celiac trunk by over 180° or an invasion of the abdominal aorta has occurred. Borderline resectable tumors are defined by tumor-induced vascular deformities involving the superior mesenteric vein or portal vein, characterized by encasement exceeding 180° or short-segment occlusions, short-segment occlusion of the hepatic artery and/or its branches, and encasement of the superior mesenteric artery less than 180°. In a metastatic stage a palliative (R)CT is recommended. In all cases the therapy should be individually discussed in a multidisciplinary tumorboard (NCCN, 2020).

Regarding adjuvant therapy after surgery a meta-analysis from Stocken et al. (2005) showed that an adjuvant chemotherapy significantly reduced the risk of death in comparison to no therapy (HR: 0.75, 95% CI: 0.64 - 0.9). Comparing two commonly used agents Gemcitabine or fluoruracil plus folinic acid (Mayo Clinic

regimen) the ESPAC-3 trial discovered no significant difference in progression free survival (PFS) or overall survival (OS) between these two adjuvant chemotherapeutic regimes (Neoptolemos et al., 2010). The PRODIGE 24/CCTG PA.6 trial, however found that patients adjuvant treated with modified (m) FOLFIRINOX (folinic acid, fluorouracil, irinotecan and oxaliplatin) had significantly better disease-free survival (DFS) and OS , but at the same time also higher toxicity, compared to an adjuvant gemcitabine treatment in primary resectable patients (Conroy et al., 2022).

The benefit of RCT in an adjuvant setting is still controversially discussed with heterogenic results in many studies (Stocken et al., 2005) and at this time German guidelines are not recommending its use (Deutsche Krebsgesellschaft, 2013). Therefore, a currently running trial, the Radiation Therapy Oncology Group (RTOG) 0848 trial, is supposed to evaluate the use of modern RCT to finalize this discussion (Abrams et al., 2020).

Neoadjuvant therapy is used to secondary attain resectability of a primary unresectable or borderline resectable tumor. About one-third of the primarily unresectable patients are able to be downsized to a resectable stage after neoadjuvant therapy (Gillen, Schuster, Meyer Zum Büschenfelde, Friess, & Kleeff, 2010). Many trials compared the two broadly used multichemo-regimens FOLFIRINOX and gemcitabine/nab-paclitaxel in clinical application. A meta-analysis of retroperspective trials showed a OS benefit for FOLFIRINOX compared to gemcitabine/nab-paclitaxel (Fatima, Alhabhbeh, Darweesh, Laswi, & Manthri, 2022). The currently running PREOPANC-2 trial was designed to verify these results in a prospective study for resectable and borderline resectable patients.

First results of a randomized phase III trial (*CONKO-007)* comparing neoadjuvant chemotherapy with RCT in patients with initially nonmetastatic unresectable PDAC could not show a significant difference in PFS or OS within both cohorts (Fietkau et al., 2022). The PREOPANC phase III trial could show that a neoadjuvant RCT with gemcitabine improves OS in resectable and borderline resectable PC compared to upfront surgery (Versteijne et al., 2022). On the other hand, the ALLIANCE A021501 phase II trial found that neoadjuvant therapy with mFOLFIRINOX was associated with a more favorable OS compared to

neoadjuvant mFOLFIRINOX plus hypofractionated radiotherapy (RT) (Katz et al., 2022).

In the end the decision must be made interdisciplinaryly for each patient considering performance status, comorbidities, and staging leading towards a highly individualized therapy (Dobiasch, Goerig, Fietkau, & Combs, 2018).

1.2. Heterogeneity in radioresistance

As described above, the use of RT in locally advanced PC is still heavily under discussion as the patient's response to RT is heterogeneous. The above-mentioned ambiguity in therapies inter alia results from the complex heterogeneity in the genetic properties of the tumor. Novel biomarkers and methods are needed to identify patient subgroups, which benefit from RT (Combs, 2015).

Radiation induces cell damage either directly through ionization of the deoxyribonucleic acid (DNA) or indirectly via reactive radiolysis products of small biomolecules (especially H_2O) DNA (Wannenmacher, Wenz, & Debus, 2013). Several inherent as well as acquired microbiological processes in the tumor are known to contribute to radioresistance. The major mechanisms are DNA damage response and repair, cell-cycle checkpoint alterations, hypoxia and the TME with its abundant stroma (Seshacharyulu et al., 2017). Several novel radiosensitizing drugs are under research in *in vitro* settings as well as in clinical trials. Nevertheless, the major obstacle on the way to clinical application and in the end improvement of OS still is the highly individual response to these therapies. This emphasizes the need for tools to identify the patient's individual best combination of RT with other therapies.

1.3. Organoids

1.3.1. History and future aspects

2D cell models have been the mainly used method in medical research due to their low costs, broad availability, as well as the possibility of fast implementation. Nevertheless, 2D cell cultures cannot hold up to the needs of personalized medicine, as major problems arise from the loss of the original phenotype due to

changes in the gene expression and the lack of mimicking the original tumor nutrition and oxygen distribution (Kapałczyńska et al., 2018). As the need for truly individualized therapy for PDAC rises, novel research platforms have been developed over the last decades. Patient-derived organoids (PDOs) have become one of the most promising technologies for fast translation of *in vitro* testing to clinical decision making (Frappart & Hofmann, 2020). A generally accepted definition of the term organoids is the following: three-dimensional cell agglomerations derived from patient's tumor material, containing multiple cell-types exhibiting the same specialized functions as the original tissue while maintaining self-renewal and organizing capacities (Lancaster & Huch, 2019). The first organoids, in the above-described sense, were generated by Sato et al. (2009) resembling intestinal villus. Since then, organoids have been generated from several different organs and entities. PDOs have the capabilities to keep the original genetic identity (Romero-Calvo et al., 2019) and can mimic the tumor's drug response *in vitro* (Tiriac et al., 2018). Thus, PDO biobanks have been developed also at the Translational Pancreatic Cancer Research Center, *Klinikum rechts der Isar of the Technical University of Munich (TUM)* to accelerate the search for biomarkers, new pharmacological targets and to finally tailor the therapy to the tumor's individual biology (Moreira et al., 2018).

1.3.2. PDOs in radiobiology

Till now the use of PDOs in radiooncology research has been very limited. The integration of organoid testing in the clinical application holds enormous potential, as we can overcome 2D cell line limitations as overestimation of response to RCT. PDOs can extend the therapeutic possibilities with extensive *in vitro* analysis for various chemoradio- as well as radioimmunotherapy combination treatments (Nagle, Plukker, Muijs, van Luijk, & Coppes, 2018). The distribution of hypoxia and the contact-effect are known to promote radioresistance and can be replicated in 3D cell models (Olive & Durand, 1994). All these advantages of the PDO-model emphasize the need for further implementation, especially in translational radiation biology.

A few relevant studies could already prove the usability of PDOs as research model for RT. Yao et al. (2020) could demonstrate that for patients with locally

advanced rectal cancer the PDOs response to chemoradiation accurately matches the clinical response and could be used as a prognostic tool.

Naumann et al. (2022) showed with a small set of four PDO lines that PDAC PDOs are feasible to evaluate treatment responses to RCT using photons as well as protons.

2. Objectives

PDAC is known to be one of the most lethal cancer entities. Despite extensive efforts in research on new therapeutics over the last decades, only little progress has been made in improving its devastating prognosis.

The reasons for treatment failure are numerous. A major aspect is the high genetic heterogeneity of PDAC which leads to an unforeseeable response to our regimens. RT is a heavily discussed modality in the neoadjuvant treatment of locally advanced pancreatic cancer, as PDAC holds a high heterogeneity in radioresistance. Various clinical studies show a divergence in the outcome after RCT and emphasize the need for novel prognostic tools.

PDOs have become a valuable research platform in oncology over the last decade, as they represent the donor's original genetic profile and contain multiple cell types that can self-organize in 3D agglomerates. This enables us to test variable treatment combinations in a highly individualized and reproducible *in vitro* setting and rapidly translate these results into clinical treatment.

In the first part of this thesis the response of PDAC PDOs to irradiation was analyzed and it was investigated if PDOs are a feasible *in vitro* platform to display the heterogeneity in radioresponse.

Above this we correlated these results with multiple radiobiological markers to characterize the underlying mechanisms for individual radioresistance and identified novel therapeutic targets to overcome radioresistance.

Furthermore, the *in vitro* results were correlated and analyzed with the corresponding patient's clinical data. The final research question was if PDOs hold the capabilities to implement a real translation of the *in vitro* results to the patient's treatment and enable us to offer highly personalized medicine in radiooncology.

3. Material and methods

3.1. Material

3.1.1. Equipment and machines

Table 3: Equipment and machines

Equipment and machine	Manufacturer	Catalog number
3-speed mini centrifuge	neoLab, Heidelberg, Germany	D-6015
Analytical balance ABS-N/ABJ-NM	Kern & Sohn, Balingen-Frommern, Germany	ABS 80-40N
Axiocam ERc 5s	Carl Zeiss, Jena, Germany	426540-9901-000
BBD 6220 CO_2 incubator	Thermo Fisher Scientific, Waltham, USA	51020241
Eismaschine (Ice machine) ZBE 70-35	Ziegra, Isernhagen, Germany	100100703v
Eppendorf Research® Plus 0,5-10 µl pipette	Eppendorf, Hamburg, Germany	3123000020
Eppendorf Research® Plus 10-100 µl pipette	Eppendorf, Hamburg, Germany	3123000047
Eppendorf Research® Plus 100-1000 µl pipette	Eppendorf, Hamburg, Germany	3123000063
Eppendorf Research® Plus 30-300 µl 8-channel pipette	Eppendorf, Hamburg, Germany	3125000052
ES Series Lab Refrigerator	Thermo Fisher Scientific, Waltham, USA	288R-AEV-TS
Gulmay RS225A Ionizing Radiation Cabinet	Gulmay Medical, Surrey, UK	
Heraeus Fresco 21 Microcentrifuge	Thermo Fisher Scientific, Waltham, USA	75002425
KS 130 basic shaker	IKA-Werke, Staufen, Germany	0002980000
Magnetic stirrers RET control-visc	IKA-Werke, Staufen, Germany	0005020000
Maxisafe 2020 Class II Biological Safety Cabinet	Thermo Fisher Scientific, Waltham, USA	51026652
Mega Star 3.0 ventilated/ refrigerated centrifuge	VWR, Darmstadt, Germany	521-1752
Multipette® M4 1µl-10ml	Eppendorf, Hamburg, Germany	4982000012
Nalgene Mr. Frosty Freezing Container	Thermo Fisher Scientific, Waltham, USA	5100-0001
Orbital shaker	GFS, Burgwedel, Germany	3015

Precision balance PCB	Kern & Sohn, Balingen-Frommern, Germany	PCB 100-3
Primovert microscope stand with binocular phototube	Carl Zeiss, Jena, Germany	415510-7144-000
Spectrophotometer Varioskan LUX	Thermo Fisher Scientific, Waltham, USA	VLBL0TD0
ThermoMixer C	Eppendorf, Hamburg, Germany	5382000015
Vortex Genie 2 vortex mixer	Scientific Industries, Bohemia USA	SI-0256
Waterbath WNB 14	Memmert, Schwabach, Germany	8419 8998

3.1.2. Consumables

Table 4: Consumables

Consumable	Manufacturer	Catalog number
12 Well Costar ® TC-Treated Plates, flat bottom, clear polystyrene	Sigma-Aldrich, St. Louis, USA	CLS3512
15 mL PP Centrifuge Tubes, CentriStar™ Cap, Sterile	Corning, Corning, NY, USA	430053
175 cm^3, 550 ml cell culture flask, PS, red filter screw cap, clear, Cellstar® TC, flat flask design, sterile	Greiner Bio-One, Frickenhausen, Germany	660175
24 Well Costar® TC-Treated polystyrene plate, flat bottom wells, sterile, lid	Corning, Corning, NY, USA	CLS3524
50 mL PP Centrifuge Tubes, Conical Bottom with CentriStar™ Cap, Sterile	Corning, Corning, NY, USA	430828
75 cm^3, 250 ml cell culture flask, PS, red filter screw cap, clear, Cellstar® TC, sterile	Greiner Bio-One, Frickenhausen, Germany	658175
96 Well White Polystyrene Microplate flat bottom clear, Tissue Culture-treated surface,	Corning, Corning, NY, USA	CLS3903
Aspiration pipette 2ml, sterile, polystyrene	Sarstedt AG & Co. KG, Nümbrecht, Germany	86.1252.011

C-Chip disposable hemocytometer, Neubauer Improved	NanoEntek, Seoul, Korea	DHC-N01
Cellstar® serologic Pipette 10 ml, sterile	Greiner Bio-One, Frickenhausen, Germany	607180
Cellstar® serologic Pipette 25 ml, sterile	Greiner Bio-One, Frickenhausen, Germany	760180
Cellstar® serologic Pipette 5 ml, sterile	Greiner Bio-One, Frickenhausen, Germany	606180
Cellstar® serologic Pipette 50 ml, sterile	Greiner Bio-One, Frickenhausen, Germany	768180
Cryo Tube 20	TPP AG, Trasadingen, Switzerland	89020
Histosette® I biopsy Processing/embedding cassetes(30 degree angle)	Simport, Quebec, Canada	M491-2
Micro tube, SafeSeal 0,5ml	Sarstedt AG & Co. KG, Nümbrecht, Germany	72.704.400
Micro tube, SafeSeal 1,5ml	Sarstedt AG & Co. KG, Nümbrecht, Germany	72.706.400
Micro tube, SafeSeal 2,5ml	Sarstedt AG & Co. KG, Nümbrecht, Germany	72.695.400
Mycoplasma Off™ 1000ml	Minerva Biolabs, Berlin, Germany	15-1000
Pipette tip, 200 µl	Sarstedt AG & Co. KG, Nümbrecht, Germany	70.30.30
Pipette tips, 1000 µl	Sarstedt AG & Co. KG, Nümbrecht, Germany	70.3050.305
Pipette tips, 20 µl	Sarstedt AG & Co. KG, Nümbrecht, Germany	70.1114

3.1.3. Chemicals and reagents

Table 5: Chemicals and reagents

Chemical/Reagent	Manufacturer	Catalog number
1M HEPES	Thermo Fisher Scientific, Waltham, USA	15630
3,3,5-Triiodo-L-Thyronine	Sigma-Aldrich, St. Louis, USA	T2877
A 83-01	Stemcell Technologies	72022
Aqua ad iniectabilia	B. Braun, Melsungen, Germany	3000970
Bovine Serum Albumine	Sigma-Aldrich, St. Louis, USA	A7030-100G
Cholera Toxin from Vibrio cholerae	Sigma-Aldrich, St. Louis, USA	C8052

Dexamethasone	Sigma-Aldrich, St. Louis, USA	D1756
Ethanol 70% (Alkopharm 70)	Brüggemann-Alcohol, Heilbronn, Germany	60870
Gibco DMEM/ F12 (1X) + L-Glutamine, +15mM HEPES	Thermo Fisher Scientific, Waltham, USA	11330-032
GlutaMAX Supplement	Thermo Fisher Scientific, Waltham, USA	35050
Human Heregulin β-1	PeproTech, Rocky Hill, USA	AF-100-03-50UG
ITS + premix	Thermo Fisher Scientific	10070791
Matrigel Basement Membrane Matrix Growth Factor Reduced	Corning, Corning, NY, USA	354230
Murine EGF	PeproTech, Rocky Hill, USA	315-09-100UG
Murine Wnt-3a	PeproTech, Rocky Hill, USA	315-20-10UG
Nicotinamide	Sigma-Aldrich, St. Louis, USA	N3376
Paraformaldehyde	Sigma-Aldrich, St. Louis, USA	P6148-500G
Penicillin-Streptomycin	Sigma-Aldrich, St. Louis, USA	P0781-100ML
Pituitary Extract bovine	Sigma-Aldrich, St. Louis, USA	P1476-2.5ML
Primocin	InvivoGen, San Diego, USA	ant-pm-1
ROCK Inhibitor (Y-27632)	Merck, Darmstadt, Germany	SCM075
Sodium hydroxid 1kg	Carl Roth, Karlsruhe, Germany	6771.1
TrypLE Express Enzyme (1X)	Thermo Fisher Scientific, Waltham, USA	12604013
Trypsin – EDTA Solution	Sigma-Aldrich, St. Louis, USA	T4299
Zeocin Selection Reagent	Thermo Fisher Scientific, Waltham, USA	R250-01

3.1.4. Buffers and solutions

Table 6: Buffers and solutions

Buffer/Solution	Manufacturer	Catalog number
Cell Recovery Solution	Corning, Corning, NY, USA	354253

Dulbecco's Modified Eagle's Medium (DMEM) – high glucose	Sigma-Aldrich, St. Louis, USA	D6429
Dulbecco's Phosphate Buffered Saline (DPBS)	Sigma-Aldrich, St. Louis, USA	D8537

3.1.5. Media

Table 7: Media

Medium	Manufacturer	Catalog number
Advanced DMEM/F-12	Thermo Fisher Scientific, Waltham, USA	12634028
Fetal bovine serum	Sigma-Aldrich, St. Louis, USA	F7524
Nu-Serum IV	Thermo Fisher Scientific, Waltham, USA	355100
PDO-Medium	Adapted from Baker, Tiriac, and Tuveson (2019) (See 3.3.5)	
R-Spondin conditioned Medium (Broutier et al., 2016, p. 1729)	(See 3.3.7)	
R-spondin growing medium	(See 3.3.7)	
R-spondin Zeocin conditioning medium	(See 3.3.7)	
Recovery™ -Cell Culture Freezing Medium	Thermo Fisher Scientific, Waltham, USA	12648-010

3.1.6. Assays and kits

Table 8: Assays and kits

Assay/Kit	Company	Catalog number
CellTiter-Glo® 3D Cell Viability Assay	Promega, Fitchburg, USA	G9682
MycoAlert® Mycoplasma Detection Kit	Lonza, Walkersville, USA	LT07-118

3.1.7. Commecial cell lines

Table 9: Commercial cell lines

Commercial cell lines	Company	Catalog number
293t-HA-Rspo1-Fc	Trevigen, Gaithersburg, USA	3710-001-K

17

3.1.8. Antibodies

Table 10: Antibodies

Antibody	Company	Catalog number
HIF-1 alpha Antibody	Novus Biologicals, Centennial, USA	NB100-479
Phospho-Histone H2A.X (Ser139) (20E3) Rabbit mAb	Cell Signaling Technology, Danvers, USA	9718S
Recombinant Anti-Ki67 antibody [SP6]	Abcam, Cambridge, UK	ab16667

3.1.9. Mouse models

Table 11: Mouse models

Mouse model	Company
Nude Mouse Crl:CD1-Foxn1nu Immunodeficient Outbred	Charles River Laboratories, Wilmington, USA

3.1.10. Software

Table 12: Software

Name	Company	Version
Aperio eSlide manager	Leica Biosystems Deer Park, USA	12.4.2.5010
Axiovision	Carl Zeiss, Oberkochen, Germany	4.8
Microsoft Excel for MacExcel	Microsoft, Redmond, USA	16.7.4
Microsoft Word for Mac	Microsoft, Redmond, USA	16.7.5
Prism 9 for MacOS	GraphPad Software, San Diego, USA	9.5.1
QuPath	The University of Edinburgh, Edinburgh, GBUK	0.3.0

3.1.11.Human samples

Table 13: Patient characteristics of the corresponding PDOs including origin, age, sex, Eastern Cooperative Oncology Group (ECOG) performance status, tumor localization. TNM, UICC, tumormarkers.

PDO ID	Origin	Age diagnosis [year]	sex	ECOG	Tumor localization	T	N	M	UICC Stadium	Resectability 1= resectable 2= borderline 3=LAPC 4=unresectable	Initial tumor marker CA19-9 [U/ml]	Initial tumor marker CEA [ng/ml]
B169	surgery	78	m	0	head	pT2	pN1 (3/41)	0	III	1	2	7.6
B188	endoscopy	69	m	0	head	ypT3	ypN1 (3/23)	0	III	3	597	2.2 NA
B211	surgery	69	m	0	head	ypT3	ypN1 (3/23)	0	III	3	597	2.2 NA
B226	radiology	61	w	0	corpus	cT4	cN+	1	IV	4	2	22.8
B283	endoscopy	64	m	0	corpus	cT4	cN0		III	3	433	0.61
B290	surgery	78	w	0	cauda	pT1c	pN2 (4/21)	0	III	1	41	5.1
B320	endoscopy	80	m	2	head	cT4	cN0	0	III	3	313	6.28
B326	surgery	71	w	1	head	pT2	pN1 (1/31)	0	III	1	24	5.8
B339	surgery	67	m	0	head	pT3	pN2 (24/33)	0	III	1	7	61.7

Table 14: Patient characteristics of the corresponding PDOs including CTx, OS and follow-up.

PDO ID	Induction CTx	Adjuvant CTx	PD (PD=1, no PD=0)	New distant metastasis	OS [months]	Cause of death 2 = alive 1 = cancer-related 0 = non cancer related 999 = unknown	last follow-up	lost to follow-up
B169	NA	Capecitabine	0	NA	43	2	31.08.2023	
B188	FOLFIRINOX (sampling before CTx)	FOLFIRINOX	1	yes	15	1	NA	NA
B211	FOLFIRINOX (sampling after CTx)		1	yes	15	1	NA	NA
B226	Gemcitabine/Paclitaxel		1	yes	3	1		
B283	FOLFIRINOX (sampling before CTx)	mFOLFIRINOX		NA	42	NA	12.06.2023	
B290	NA	Gemcitabine,	1	yes	21	1	NA	NA
B320	NA				1	NA		22.06.2020
B326	NA	mFOLFIRINOX	0	NA	36	2	12.05.2023	NA
B339	NA	mFOLFIRINOX	0	NA	3	NA	27.10.2020	

3.2. Study approval

The collection of PDOs and use for this study was approved by the ethics committee of the TUM (protocol code 373/20 S-EB from 13 July 2020). A written informed consent of all patients for research use was obtained prior to sample acquiring.

3.3. Cell culture methods

The following procedures were performed under a sterile laminar flow hood. The methods were adapted from Dantes et al. (2020).

The incubator (BBD 6220 CO_2 incubator) was set by default at 37 °C, 5% CO_2 and 95% humidity.

3.3.1. Organoid generation

Already isolated PDOs were obtained from the Patient-derived Organoid Unit within the Translational Pancreatic Cancer Research Center (Center Head: Prof. Max Reichert), Medical Clinic and Polyclinic II at the TUM. PDOs were either isolated from fine needle aspiration or surgery specimens.

3.3.2. Culturing of PDOs

The PDOs were cultured in 24 well TC-treated, flat bottom embedded in a Matrigel-dome and surrounded by PDO-medium (1.4.5). After microscopic control the PDOs were passaged every one to two weeks, if either the confluence reached 70-80%, single organoids were bigger than 20% of diameter of the Matrigel-dome, the Matrigel-dome was getting instable or central necrosis was observed.

For splitting, the medium was removed from each well. Each well was rinsed with 1 ml DPBS and the supernatant was discarded. 250 µl Cell Recovery Solution (CRS) was added in each well. A 15 ml centrifuge tube was filled with 8 ml 4°C cold DPBS. The Matrigel of each well was dissolved with 1 ml DPBS from this falcon by gently pipetting up and down with a 1000 µl pipet tip. The solution was transferred back into the 15 ml falcon. Then the falcon was chilled on ice for 30 minutes (min), while inverting it every 10 min. Afterwards the sample was

centrifuged at 1000 revolutions per minute (rpm) at 4°C for 5 min. The supernatant was discarded, 8 ml cold DPBS was added, and the falcon was centrifuged with the same parameters. The supernatant was removed and the cell pellet was resuspended with 50 µl 0°C cold Matrigel for each new well. The sample was put back on ice. The ratio for splitting in general was 1:2, but was adjusted regarding the size and number of organoids in the Matrigel-dome. A 37 °C prewarmed 24 well TC-treated flat bottom plate was put on a 37°C prewarmed 150 cm^3 cell culture flask, which was filled with sterile water. The prewarming ensured a fast hardening of the Matrigel and prevented the dome from flattening. 50 µl of the Matrigel cell pellet mix were carefully pipetted in the middle of the well with a precooled 200 µl pipet tip and a hemisphere was formed (depicted in Figure 1). The plate was put in the incubator for 10 min. PDO-medium (See 3.3.5) was supplemented with 15,2 µMol/l Rho Kinase Inhibitor (ROCK-inhibitor) and 500 µl PDO-medium was added to each well and the plate was put in the incubator for cultivation.
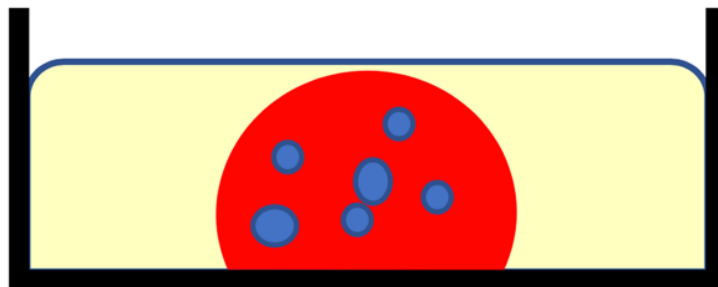
Figure 1: Simplified graphic of the profile of a well with organoids (blue) embedded in Matrigel (red) surrounded by medium (yellow).

3.3.3. Cryopreservation

For long term storage in a liquid nitrogen tank at a temperature of -196 °C the PDOs were prepared following the instructions below. The cells were used for cryopreservation when they had grown to 70-80 % confluence in the 24 well culturing plates. The medium was aspirated from each well and 1 ml room-temperature warm DBPS was carefully added and aspirated to wash away media residues. 250 µl Cell Recovery Solution was added. A 15 ml tube was filled with 8 ml 4°C cold DPBS. 1 ml of this DBPS was added to each well and the Matrigel was dissolved by slowly pipetting up and down with a 1000 µl pipet tip. The

mixture containing Matrigel, DBPS and CRS was transferred to the 15 ml tube. Each well was again washed with 1 ml of the mixture from the 15 ml tube, to make sure no organoids were remaining on the plate. The tube was put on ice for 45 min. Then the sample was centrifuged at 1000 rpm at 4°C for 5 min. The supernatant was aspirated to 2 ml. The centrifuge tube was filled to 8 ml with 4°C cold DBPS and resuspended. The falcon was centrifuged again with the same parameters. The supernatant was discarded carefully without touching the cell pellet. The pellet was dissolved with 1ml/well Recovery Cell Culture Freezing Medium. The solution was transferred into 1.5 ml cryovials . The cryovials were put into a Mr. Frosty™ freezing container filled with 100% isopropyl alcohol guaranteeing a constant cooling rate of -1°C/min. The freezing container was put into a -80°C freezer for at least 24 hours (h) and then transferred to the liquid nitrogen tank.

3.3.4. Thawing

The cryovial was warmed until it started to become liquid. The sample was transferred into a 15 ml centrifuge tube filled with 8 ml 37°C prewarmed DMEM high glucose. The tube was centrifuged at 1000 rpm at 4°C for 5 min. The supernatant was aspirated carefully without touching the pellet and 8 ml 4°C cooled DPBS were added. The cell pellet was resuspended and the tube was again centrifuged with the same parameters. The supernatant was discarded and 50 µl Matrigel per well were added. The following steps correspond to 3.3.2.

3.3.5. PDO-medium

The PDO-medium for culturing and experiments was not commercially available. It was generated following the instructions below. Due to the instability of some of the reagents, the PDO-medium was used within a maximum of two weeks. The following reagents were mixed and stored at 4°C in 15 ml aliquots.

Table 15: PDO medium components and final concentrations.

Component	Concentration in final medium
Gibco DMEM/ F12 (1X) + L-Glutamine, +15mM HEPES	88.5 %vol
D-Glucose	5 mg/ml
ITS + premix	0.5 %vol

3,3,5-Triiodo-L-Thyronine	5 nM
Dexamethasone	1 µM
Cholera Toxin	100 ng/ml
Penicillin/Streptomycin	1 %vol
Nu-Serum IV	5 %vol
Murine EGF	20 ng/ml
Bovine Pituitary Extract	25 µg/ml
Nicotinamide	10 mM
A83-01	0.5 µM
R-Spondin conditioned medium	5 %
Human Heregulin β-1 (Neuregulin)	100 ng/ml

3.3.6. Medium Change

A medium change was carried out whenever the PDO-medium turned its color from red-orange into a light pink-yellow, the Matrigel-dome was not surfaced with medium or the last medium change was more than a week ago. The old medium was aspirated and exchanged with 500 µl fresh PDO-medium. The addition of ROCK-inhibitor was only necessary after passaging, in which the PDOs have suffered cellular stress due to mechanical irritation.

3.3.7. R-spondin conditioned medium

R-spondin conditioned medium is an essential component of the PDO-medium and was produced in our lab. Firstly, a growing and a conditioning medium was produced and stored at 4°C.

R-spondin growing medium:

Table 16: Components of the R-spondin growing medium.

Component	Amount
Gibco DMEM/ F12 (1X)	500 ml
Heat activated FBS	60 ml
Penicillin/Streptomycin	5 ml

R-spondin conditioning medium:

Table 17: Components of the R-spondin conditioning medium

Component	Amount
Gibco DMEM/ F12 (1X)	500 ml

Penicillin/Streptomycin	5 ml
1M HEPES	5 ml
GlutaMAX Supplement	5 ml

One cryovial of 293t-HA-Rspo1-Fc cells was dissolved in 37°C prewarmed 9.5 ml R-spondin growing medium in a 15 ml tube. The falcon was centrifuged at 700 rpm at room temperature for 5 min. The supernatant was discarded, and the cell pellet was resuspended with 1 ml R-spondin growing medium. 50 ml R-spondin growing medium were filled into a 175 cm^3 cell culture flask. First 3 µl/ml (150 µl) zeocin selection reagent and then the cell suspension was added to the cell culture flask. The cells were incubated for two to four days until they reached 80% - 90% confluency.

Then the medium was aspirated. The flask was washed with 25 ml room temperature DPBS and the DPBS was discarded. 2 ml Trypsin-EDTA solution was added and the flask was incubated for 3-5 min at 37°C. The cells were resuspended with 18 ml R-spondin growing medium and transferred into a 50 ml centrifuge tube. The tube was centrifuged at 700 RPM at room temperature for 5 min. Then the supernatant was aspirated and 6 ml R-spondin growing medium was added. Six 175 cm^3 were filled with 50 ml R-spondin growing medium. 1 ml of the cell suspension was added to each flask. To one of the six flasks, the "selection flask", 150 µl Zeocin Selection Reagent was added. The flasks were incubated for two to four days until the cells were confluent.

The following applies to all but the selection flasks. The medium was discarded and washed with 25 ml room temperature DPBS twice. 50 ml R-spondin growing medium were added to each flask. And the cells were incubated for one week. After one week the conditioned medium was transferred into 50 ml centrifuge tubes. The tubes were centrifuged for 5 min at room temperature at 1000rpm. Then the medium was sterile filtered with a 2 µm filter and aliquoted. The R-spondin conditioned medium was stored in -20°C freezer.

The selection flask was used to repeat the steps if more R-spondin conditioned medium was needed

3.3.8. Mycoplasma testing

PDOs were regularly tested for mycoplasma contamination. Therefore, 2-3 wells for each PDO were cultivated in a penicillin-streptomycin free PDO-medium for two passages. One week after the second passage 1 ml of the medium supernatant was collected in a 1.5 ml micro tube.

The test was performed with the *MycoAlert® Mycoplasma Detection Kit*. The procedure follows the original instructions for use by Lonza (2012). The micro tube was centrifuged for 5 min at room temperature with 200 G. 100 µl supernatant of the centrifuged medium were transferred into a well on a 96 well plate. 100 µl negative and positive control were pipetted in one well each. 100 µl *MycoAlert Reagent* were added to each well and incubated for 5 min. Then the luminescence of the three wells was measured, according to the manufacturer's parameters, with the spectrophotometer *Varioskan LUX* and saved as measurement A. 100 µl *MycoAlert substrate* were added per well and incubated for 10 min. The luminescence was measured with the same parameters and saved as measurement B. The results of the corresponding wells of measurement B were divided by measurement A. A value from 0-0.9 implies negative, >1.2 positive. The threshold between 0.9 and 1.2 led to a repetition after another passage.

3.4. Radiobiological methods

3.4.1. Experimental setup for determination of the radioreponse

The PDOs' response to RT was determined using a cell viability assay (see 3.4.4). Two different approaches, with two different time points (72 h and 7 days after RT) of the cell viability assay, were performed (Figure 2). Except for the time points the setup was identical. 5 plates with 5 replicates each were used. For all approaches 5000 cells per well were solved in 50 µl Matrigel. After 24h the plates were irradiated with doses of 0 Gray (Gy), 2 Gy, 4 Gy, 6 Gy and 8 Gy. 72 h or respectively 7 days after irradiation a microscopic evaluation and afterwards a cell viability assay was performed.

Figure 2: Experimental *in vitro* setup for analysis of the PDOs' radioresponse. PDOs were irradiated 24h after seeding. Cell viability read out was performed at two different time points.

3.4.2. Seeding

The *in vitro* experiments were carried out in 96 well white, polystyrene, flat, clear bottom, tissue culture-treated surface microplates. The PDOs were used for experiments if they reached a confluence from 70-80 %. The procedure followed the passaging for cell culture (see 3.3.2) up to the generation of the cell pellet. Afterwards, the supernatant was discarded and 4 ml TrypLE Express Enzyme 1x for enzymatic separation of the cells was added. The suspension was incubated for 5 min in a 37°C warm water bath. To stop the enzymatic separation 5 ml warm DMEM high glucose was added and the sample was centrifuged at 1000 rpm at 4°C for 5 min again. The supernatant was aspirated except for 1 ml. The sample was resuspended and 10 µl of the suspension was given into four separate Neubauer improved counting chambers each without the use of trypan blue. The cells were manually counted. The number of cells per ml was calculated with the following formula:

$$\frac{counted\ cells}{4} \times 10{,}000 = \frac{cells}{ml}$$

For each experiment, five 96 well plates with 5 replicas per plate and 5000 cells for each replicate were prepared. The cell suspension was centrifuged at 1000 rpm at 4°C for 5 min. The supernatant was carefully aspirated without destroying the cell pellet. Matrigel (10 µl per well) was added to the cell pellet and resuspended. The suspension was put on ice. 10 µl of the Matrigel cell mixture was carefully pipetted with a precooled 20 µl pipette tip in the middle of each well of the prewarmed 96 well plates. The plates were placed in the incubator for 15 min. Afterwards, 15.2 µMol/l ROCK-inhibitor were added to the 37°C prewarmed PDO-Medium. 100 µl PDO-medium were added gently to every well. To all wells that were not filled with PDO-Matrigel-domes 100 µl DPBS were added to prevent medium evaporation. The plates were placed in the incubator.

3.4.3. Cell irradiation

The cells were irradiated with 0 Gy, 2 Gy, 4 Gy, 6 Gy and 8 Gy using the *Gulmay RS 225A* Ionizing Radiation Cabinet. The irradiation was performed at 200 kV and 15 mA using a 5 mm copper filter. The distance between the collimator and the rotating tablet was set to 500 mm. These settings resulted in a dose rate of 1:07 min/Gy. To ensure that all cells undergo the same conditions, the 0 Gy control group was also carried from the incubator to the room of the radiation cabinet. The time outside the incubator was kept as short as possible and varied between 30-40 min.

3.4.4. Cell Viability Assay

The cell viability was measured 72 h or 7 days after irradiation with the *CellTiter-Glo® 3D Cell Viability Assay*. The procedure was adapted from the technical manual (Promega, 2015). The assay lyses the cells and the Matrigel. The ATP of the viable cells is bound by a luciferase, an enzyme capable of transducing ATP into light emission. The emitted light is directly proportional to the amount of ATP and therefore also proportional to the viable cells in the probe (Bach, 2019).

CellTiter-Glo® 3D reagent was thawed over night at 4°C in the fridge. The plates with the prepared PDOs and the reagent were tempered at room temperature for 30 min before adding the reagent. Then 100 µl *CellTiter-Glo® 3D* reagent was added to every well with PDO-Matrigel-domes. The plates were put on the orbital shaker for 5 min to enhance cell lysis. Afterwards, the cells were incubated at room temperature for 25 min. The ATP-luciferase signal was read out with the *Spectrophotometer Varioskan LUX* (Thermo-Fisher) in luminescence mode and the raw data was saved in Excel (Microsoft).

3.4.5. Microscopic analysis

The morphology, size and number of PDOs were evaluated via phase contrast microscopy with the *Primovert microscope* (Carl Zeiss). Photos of the samples were taken using the microscopic camera *Axiocam ERc* (Carl Zeiss) in 4x and 10x magnification with the corresponding software *Axiovison* (Carl Zeiss). The mean organoid area was measured manually using the bioimage analysis open-source software "QuPath" (The University of Edinburgh). Representing replicates

for each PDO at all doses were chosen and the mean area of 15 single organoids in these replicates was calculated.

3.4.6. Immunohistochemical staining

The immunohistochemical (IHC) staining and embedding were performed in collaboration with the Institute of Pathology/Comparative Experimental Pathology of the TUM. The PDOs were regularly passaged in 24 well TC-treated, flat bottom plates (see 3.3.2) When the organoids reached about 80% confluency, they were irradiated with doses of 0 Gy, 4 Gy and 8 Gy. The time points for fixation after irradiation varied between the desired staining. For γ-H2ax staining, which was used to quantify DNA double strand breaks (DSBs) (Rogakou, Pilch, Orr, Ivanova, & Bonner, 1998), organoids were fixed 1 h after irradiation. PDOs stained for Hypoxia-inducible factor 1α (HIF-1α), which is upregulated as a response to hypoxia (Elzakra & Kim, 2021), and Ki-67, a protein only detectable in proliferating cells (Gerdes et al., 1984), were fixed 24 h after irradiation. The PDOs were fixed with formalin 4% and incubated at room temperature for 2 h. The formalin was carefully aspirated and the Matrigel-domes, carrying the organoids, were transferred into embedding cassettes. The cassettes were placed into a container filled with ethanol 70%, afterwards embedded in paraffin and cut in 2 µm thick slices. IHC was performed and standardized by the fully automated research staining machine BOND RX (Leica Biosystems) according to the manufacturer's instruction. All slides were scanned with a digital pathology slide scanner "Aperio AT2".
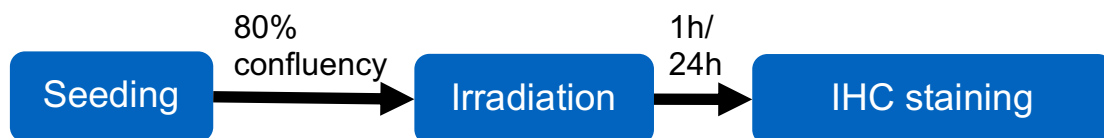

Figure 3: Experimental *in vitro* setup for IHC staining for γ-H2ax (1h time point), HIF-1α (24h time point) and Ki-67 (24h time point). PDOs were irradiated (0 Gy, 4 Gy, 8 Gy), when organoid formation was completed and a confluency of about 80% was reached.

3.4.7. Evaluation of IHC

The stained slides were electronically available via the *Aperio eSlide manager* (Leica Biosystems). A quantitative evaluation of the staining was performed with *QuPath*. (Bankhead et al., 2017). The tool "positive cell detection" was used with

setup parameters set on optical density sum to detect the positive stained cell nuclei for γ-H2ax and Ki-67. The other parameters for the respective staining were adjusted manually for optimal cell detection. The measurement for HIF-1-α was also accomplished with QuPath by manually training a multi variable random tree object classifier.

3.5. Molecular biological methods

3.5.1. RNA harvesting, isolation and sequencing

Ribonucleic acid (RNA) harvesting of the PDOs was performed by the Patient-derived Organoid Unit within the Translational Pancreatic Cancer Research Center (Center Head: Prof. Max Reichert), Medical Clinic and Polyclinic II at TUM. For this, PDOs were cultivated in 24 well plates and further processed, according to the working groups protocols, when they reached a confluency of about 80%. The RNA containing solution was transferred to micro tubes with RLT buffer and ß-mercaptoethanol and stored in a -80°C freezer. RNA isolation was performed using the RNeasy Mini Kit (Quiagen) following the manufacturer's protocol, followed by RNA-sequencing.

3.5.2. RNA analysis

RNA analysis was performed in cooperation with the Patient-derived Organoid Unit within the Translational Pancreatic Cancer Research Center (Center Head: Prof. Max Reichert), Medical Clinic and Polyclinic II at TUM:

Genome-wide differential gene expression analysis was calculated using the DESeq2 R package (Love, Huber, & Anders, 2014) applied to RNA-sequencing count data from PDO lines. A false discovery rate (FDR) of < 0.1 was considered significant. Phenotype specific contrasts were generated per sample using information on radiosensitivity class (resistant, intermediate and sensitive).

For gene set enrichment analysis (GSEA) of one versus rest differential gene expression signatures (GES) comparisons were calculated for each radiosensitivity class (resistant, intermediate and sensitive) versus all other samples using DESeq2 for RNA count data as described above. These radiosensitivity-specific GES were represented by Wald test statistics per gene

and were interrogated by GSEA (Subramanian et al., 2005) (Korotkevich et al., 2021) using the HALLMARK gene set collection from MSigDb version 7.4 (Liberzon et al., 2015). The resulting normalized enrichment score (NES) matrix with HALLMARKS in rows and radiosensitivity-specific one vs. rest signatures in columns was illustrated using the pheatmap R package (Kolde, 2019).

For GSEA of individual contrasts of the radionsensitivity classes (e.g. resistant vs. sensitive), the respective Wald stat GES was interrogated using HALLMARK gene sets as well as subtype specific gene sets retrieved from the supplement of Moffitt et al. (2015), i.e. the top 100 genes from the basal-like and classical factor, respectively. Normalized enrichment scores were calculated using analytic rank-based enrichment analysis (Alvarez et al., 2016). Enrichment and leading edge results were illustrated using custom Python scripts.

3.6. In vivo methods

An orthotopic xenograft mouse model was performed for *in vivo* validation. PDOs were harvested over several weeks to ensure a sufficient number of cells for the implantation. In the first experimental setup 500.000 cells were resuspended with 50 µl Matrigel for each mouse and orthotopically implanted in the pancreatic tissue of thymus aplastic Crl:CD1-Foxn1 nude mice. After 6 weeks, the mice were controlled weekly for tumor growth with MRI (Mediso nanoscan PET/MR 3T).

The same experimental setup was repeated with the orthotopic injection of one million cells per mouse to improve the rate of sufficient tumor growth.

3.7. Clinical data

Clinical patient data was collected using the clinical workstation system at the Klinikum rechts der Isar, Technical University Munich.
The relative cell viability of the PDOs was compared with different variables like overall survival (OS), occurrence of metastasis, tumor stage or the initial serum level of CA-19.9.

3.8. Statistical methods

Cell viability assays were performed at least three times in independent experiments with five replicates for each dose. The effects of irradiation on cell viability as well as on the expression on the different IHC markers were analyzed using two-sided t-tests. Correlation was tested with Pearson's R coefficient. Statistical tests and graph plotting were carried out using GraphPad Prism 9.5.1 (GraphPad Software, Inc). P values < 0.05 were considered significant.

The statistical analysis of the RNA-data set is explained in 3.5.2.

4. Results

4.1. Heterogeneity in radio-response

4.1.1. Morphology of PDOs after irradiation

The included PDOs in general form spherical 3D structures sharply defined against the surrounding area. The characteristics of these structures varied between the different PDO lines. They partly formed cystic organoids lined with a cell monolayer. Also, solid forms completely consisting of cells as well as organoids with a central cell agglomeration surrounded by fluid followed by a cell layer have occurred. These characteristics were constant within one PDO line. Cells having contact with the bottom of the plate showed a 2D growth resembling classical PDAC colony forming assays.

In light microscopy, the different PDO-lines showed heterogeneity in the growth behavior after irradiation (Figure 4). The size, the number and the morphology showed a correlation with increasing irradiation doses. At higher doses, the organoid diameter was getting smaller, organoids partly looked burst, losing their sharp outer layer and spheric structure.
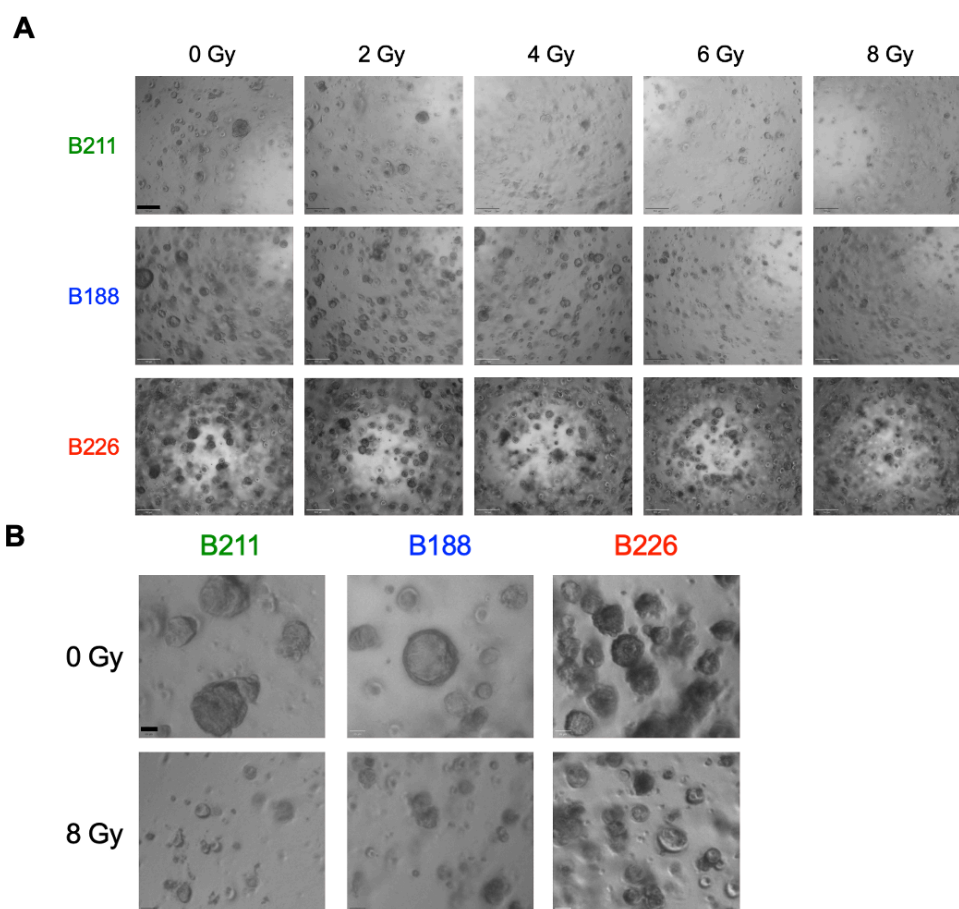
Figure 4: A: Light microscopy one week after irradiation of three different PDO-lines after five different irradiation doses. Color scheme depicts the radiosensitivity classes (4.1.5). Scale bar = 100 µm. **B:** The same PDOs after application of doses of 0 Gy and 8 Gy are depicted in a higher magnification. Scale bar = 20 µm.

4.1.2. Radio-response 72h after irradiation

To analyze the response of PDOs to irradiation, a 3D cell viability assay was performed 72 h after irradiation (96 h after seeding) with 11 PDO-lines (Figure 5 A). Only a part of the PDOs showed a dose-dependent decrease in growth. A significant difference between the proliferation could not be observed at any dose. A half maximum inhibitory dose (D_{50}) could not be reached for any PDO line using a maximum dose of 8 Gy. B290 showed the nominally highest relative response to irradiation with 74.1% at 8 Gy in comparison to an average of 104.35% within all 11 lines. The proliferation of many PDO lines rose above 100% after irradiation in comparison to the individual proliferation at 0 Gy, questioning the meaningfulness of the experimental setup. Figure 5 B depicts the PDOs

34

contained only in the radiosensitivity classes (see 4.1.5) at the 72h readout time point.
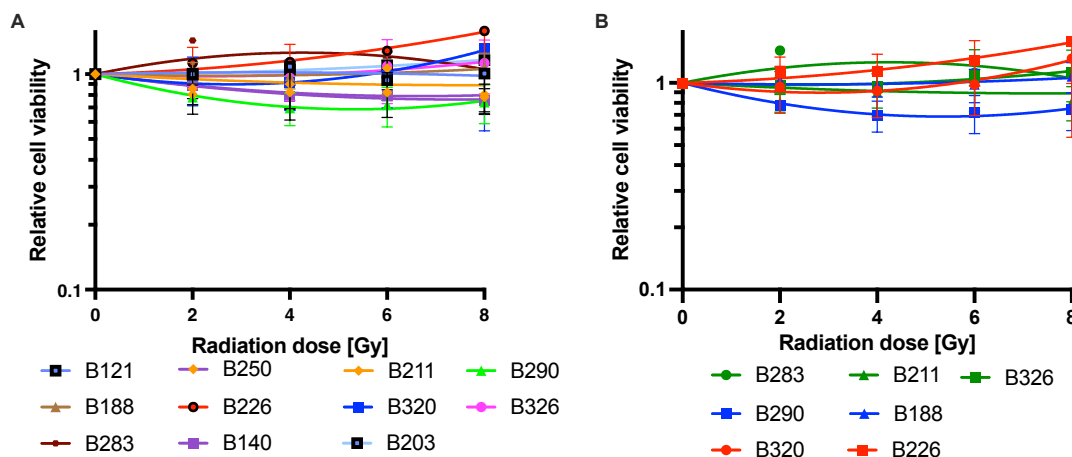

Figure 5: A: Nonlinear fit of the relative cell viability of seven different PDOs 72h after irradiation with 0, 2, 4, 6, 8 Gy normalized to 0 Gy. D_{50} could not be reached for any PDO line. **B:** Nonlinear fit of the relative cell viability of seven different PDOs included in the in 4.1.5 described radiosensitivity classes 72h after irradiation with 0, 2, 4, 6, 8 Gy normalized to 0 Gy. Color scheme depicts the radiosensitivity classes. Data in A and B is shown as the mean of 3 independent experiments Error bars represent standard deviation (SD).

4.1.3. Radio-response using higher irradiation dose

To investigate if a higher dose was necessary to create a sufficient decrease in cell viability a maximum dose of 16 Gy was applied for three different PDOs. Again, the D_{50} was not reached with a relative cell viability of 57.28% (B188 at 16 Gy) being the strongest response to irradiation (Figure 6). For B326 the relative cell proliferation was again above 100% indicating that at this time point other factors seem to have an influence on the proliferation, taking into account that the number of cells is equalized.
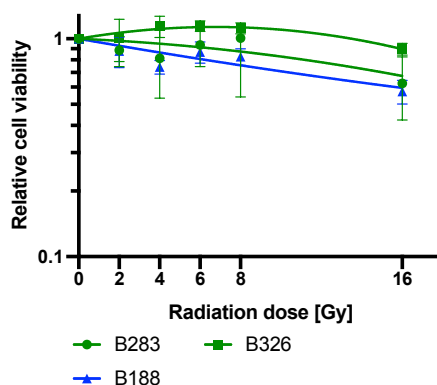

Figure 6: Nonlinear fit of the relative cell viability of three different 72h after irradiation with additionally 16 Gy. All values are normalized to the 0 Gy cell viability of the corresponding PDO. D50 could not be reached for any PDO line. Color scheme depicts the radiosensitivity classes (4.1.5). Data is shown as the mean of 3 independent experiments Error bars represent SD.

4.1.4. Radio-response comparing different timepoints

In order to better display the heterogeneity in cell viability after RT in addition to to the 72h timepoint, a one- and two-week timepoint after irradiation was established, by again using the cell viability assay. Two PDO lines were irradiated with 8 Gy and the cell viability assay was performed after 72h, one week and two weeks (Figure 7). The attenuation of the relative cell viability was distinctly higher both one-week and two-weeks after irradiation than compared to the 72h timepoint. There also was a higher difference between the different PDO lines at the same timepoints compared to 72h, being almost three-fold the value for the one-week time point (Δ B188/B283 72h: 0.075%, 1 week: 0.203%, 2 weeks: 0.28%).By taking the higher time consumption into account, the one-week timepoint was selected for the further experimental setup.
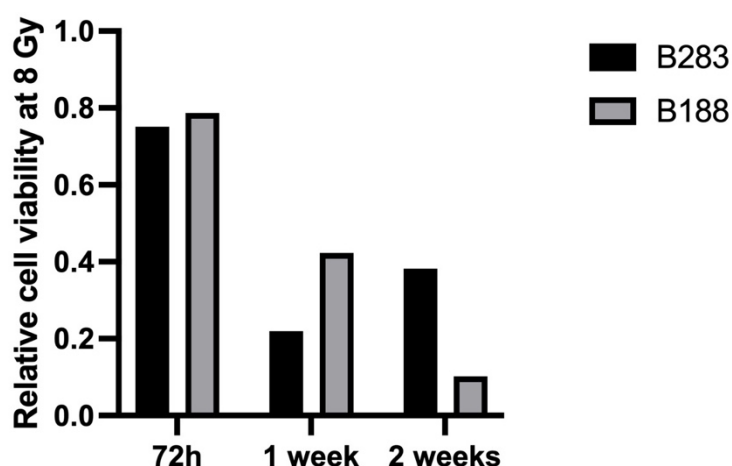

Figure 7: Columns depict the relative cell viability at 8 Gy measured 72h, 1 week and 2 weeks after irradiation with 8 Gy. All values are normalized to the 0 Gy cell viability of the corresponding PDO.

4.1.5. Radio-response one week after irradiation

Comparing a larger number of PDO lines, the variability in cell viability between the PDOs was still more pronounced at the one-week time point (Figure 8). The relative cell viability varied from maximum 0.836 ($\pm$ 0.168, B226) to minimum 0.313 ($\pm$ 0.073, B283) at 8 Gy. For all cell lines the relative proliferation was getting smaller anti-proportional to the applied dose (Figure 8).
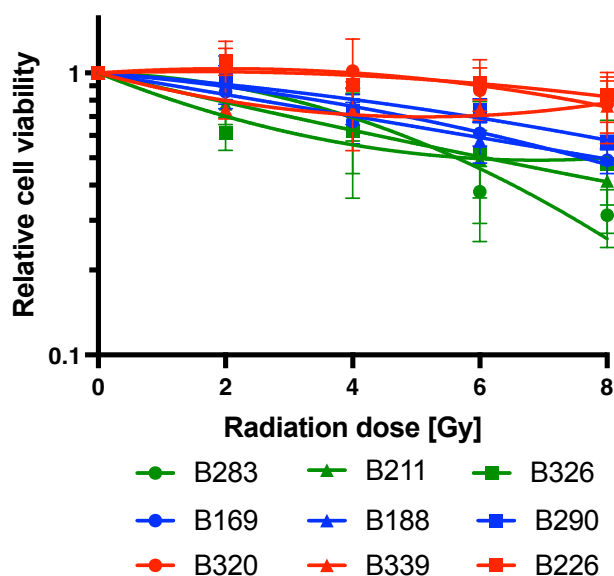
Figure 8: Nonlinear fit of the relative readioresponse (normalized to 0 Gy) of nine different PDOs measured with CellTiter-Glo®
3D Cell Viability Assay one week after irradiation with 0, 2, 4, 6, 8 Gy. Adapted from Cadacio (2021). Color scheme depicts the
below described radiosensitivity classes. Data is shown as the mean of 3 independent experiments Error bars represent SD.

To measure and display the differences in the relative cell viability, the area under
the curve (AUC) was calculated (Figure 9) and compared with the relative cell
viability at 8 Gy (Figure 10). Since the drop in cell viability occurred at higher
irradiation doses, the AUC could not significantly display the heterogeneity,
nevertheless a trend similar to the results of the 8 Gy cell viability was visible.
Therefore, the relative cell viability at 8 Gy was used for further analyses.
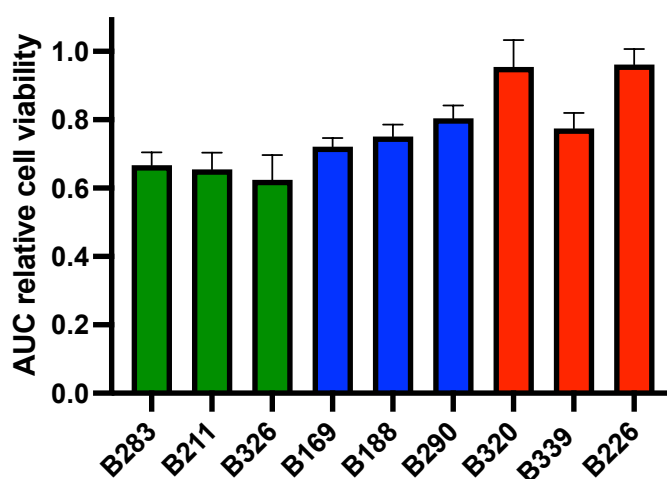

Figure 9: AUC of the relative cell viability (normalized to 0 Gy) of nine different PDO lines one-week after irradiation with 8 Gy.
PDO color scheme and sorting from left to right is according to the below described radiosensitivity classes. There is no significant
difference in between the radiosensitivity subgroups. Data is shown as the mean of 3 independent experiments. Error bars
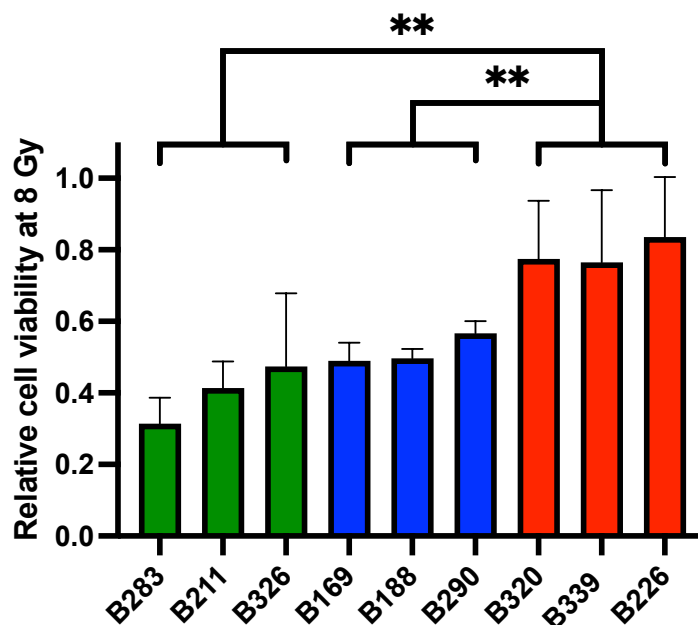represent SD.

Figure 10: Relative cell viability at 8 Gy (normalized to 0 Gy) of nine different PDOs one week after irradiation. PDO color scheme and sorting from left to right is according to the below described radiosensitivity classes. Sensitive vs. resistant subclass and intermediate vs resistant subclass show significantly different mean relative cell viability (**=p<0.01). Data is shown as the mean of 3 independent experiments. Error bars represent SD.

To simplify the comparison of the PDOs subclasses were formed, according to the relative proliferation at 8 Gy measured with the CellTiter-Glo® 3D Cell Viability Assay:

Sensitive: B283, B211, B326
Intermediate: B169, B188, B290
Resistant: B320, B339, B226

The subclasses showed a significant difference in cell viability at 8 Gy between resistant and sensitive as well as between the resistant and the intermediate PDO subgroup (Figure 10).

The relative mean organoid area showed a similar distribution as the relative cell viability (11 A) with a noticeable but non-significant (Pearson's R = 0.6307, p = 0.0686) correlation between the PDOs' cell viability at 8 Gy and the mean organoid area at 8 Gy (11 B). The comparison between the sensitive and resistant radioresponse cell viability subclass showed a significant difference in the relative mean organoid area after RT with 8 Gy (p < 0.05, Figure 12).
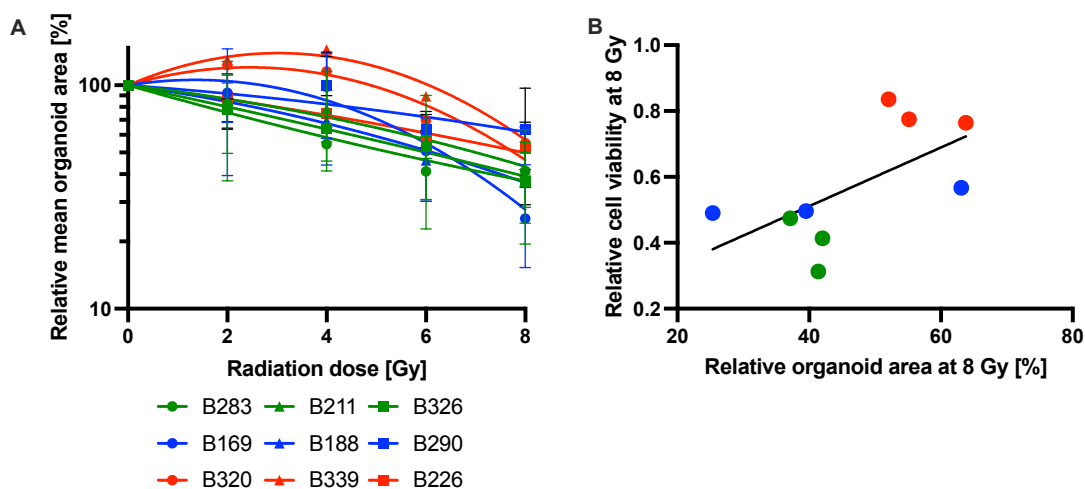
Figure 11: A: Nonlinear fit of the relative organoid area at 8 Gy (normalized to 0 Gy). There was a significant difference between the mean area of the sensitive and the resistant subclass (*=p<0.05). PDO color scheme and sorting from left to right is according to the above described radiosensitivity classes. Data is shown as the mean of 3 independent experiments except for B326 (n=2) and B339 (n=1). Error bars represent SD. **B:** Scatter plot graph with linear regression of relative cell viability at 8 Gy and relative cell organoid area at 8 Gy visualizes the trend towards a positive correlation (Pearson's R=0.6307, p=0.0686). Color scheme is according to the above described radiosensitivity classes.
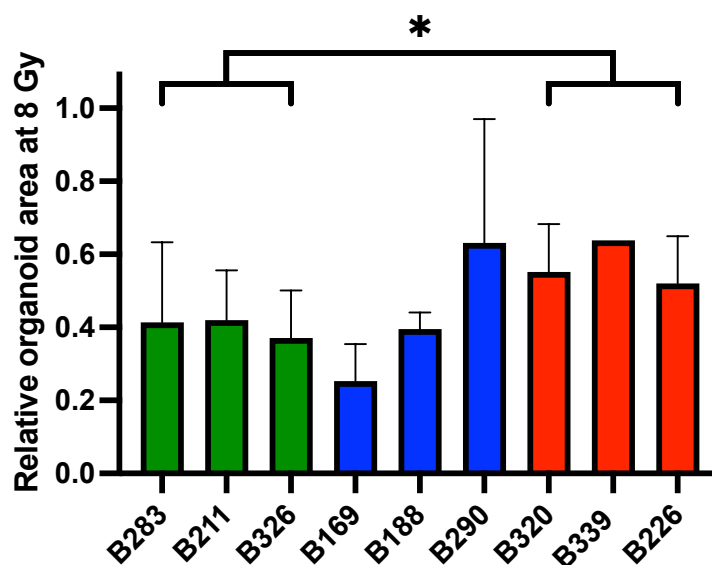

Figure 12: Relative organoid area at 8 Gy (normalized to 0 Gy). There was a significant difference between the mean area of the sensitive and the resistant subclass (*=p<0.05). PDO color scheme and sorting from left to right is according to the above described radiosensitivity classes. Data is shown as the mean of 3 independent experiments except for B326 (n=2) and B339 (n=1) Error bars represent SD.

4.2. Radiobiological characterization by IHC

4.2.1. DNA-damage (γ-H2ax)

To investigate radiation induced DNA DSBs PDOs were fixed 1 h after irradiation and stained for γ-H2ax (Figure 13 B). Comparing the mean of all PDO lines there was a significant increase of γ-H2ax positive cells after irradiation (0 Gy vs 4 Gy and 0 Gy vs 8 Gy, *p<0.001*). No significant difference between 4 Gy and 8 Gy was measurable: The mean of positive stained cells with a dose of 4 Gy is 87.66% (SD 10.52%) compared to 89.49% (SD 5.48%) at 8 Gy.

Opposing the levels of positive stained cells of the radiosensitive with the radioresistant cell viability subgroup at 8 Gy, the sensitive subgroup had significantly higher levels (sensitive: 96.34% SD 2.065%, resistant: 86.68% SD 2.889%, *p=0.0092,* Figure 13 A). These findings imply that a higher amount of DNA DSBs might be an indicator for increased radiosensitivity.
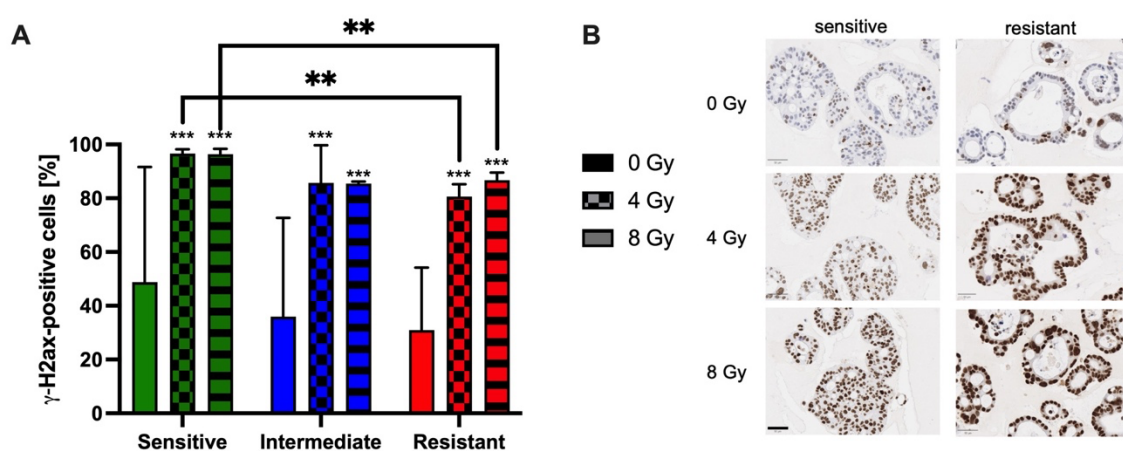

Figure 13: A: Comparison of the mean percentage of γ-H2ax positive stained cells of the 3 radiosensitivity subgroups after irradiation with 0 Gy, 4 Gy and 8 Gy. Color scheme and sorting from left to right is according to the above described radiosensitivity classes. There was a significant difference between the mean of all PDOs at 0 Gy and 4 Gy as wells as between 0 Gy and 8 gy (*** above bars=p<0.001). There was a significant difference between sensitive and resistant subgroup at 4 Gy (**=p<0.01) and at 8 Gy (**=p<0.01). Error bars represent SD. **B:** γ-H2ax staining 1h after irradiation with 0 Gy, 4 Gy and 8 Gy of representative PDOs from the sensitive and the resistant subgroup showing the increase of γ-H2ax positive cells after irradiation. Scale bars equal 50 µm.

4.2.2. Proliferation (Ki-67)

The organoids were fixed 24h after irradiation for Ki-67 to quantify the number of cells in proliferation (Figure 14 B). Positively stained cells had a low variability

within each cell line after application of 0 Gy, 4 Gy and 8 Gy. The SD of the mean of the three doses for each PDO varied between 4% to 13%. No trend towards a rise or decline of the proliferation marker after irradiation was identifiable. There was a significant (*p=0.0426*) higher amount of Ki-67 positive stained cells comparing the baseline (0 Gy) of the sensitive subclass with the baseline of the intermediate and resistant subclass (Figure 14 A). These results indicate that Ki-67 staining might be used for predicting radiosensitivity.
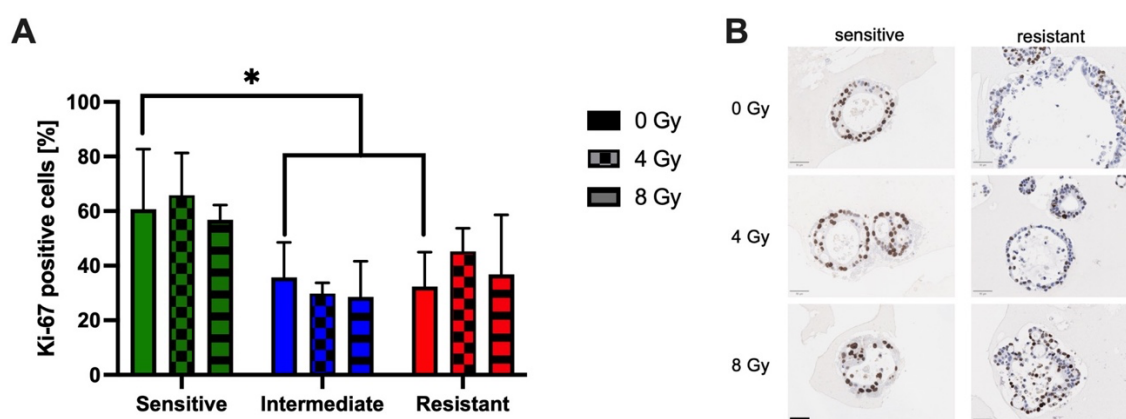

Figure 14: A: Comparison of the mean percentage of Ki-67 positive stained cells of the 3 radiosensitivity subgroups after irradiation with 0 Gy, 4 Gy and 8 Gy. Color scheme and sorting from left to right is according to the above described radiosensitivity classes. There was a significant difference baseline between the mean of the sensitive subgroup and the mean of intermediate + resistant subgroup at 0 gy(*=p<0.05). Error bars represent SD.**B:** Ki-67 staining 24h after irradiation with 0 Gy, 4 Gy and 8 Gy of representative PDOs from the sensitive and the resistant subgroup. The resistant subgroup shows a lower amount of positive stained cells (brown nuclei) at all doses. Scale bars equal 50 µm.

4.2.3. Hypoxia (HIF-1α)

The staining of HIF-1α did not show significant changes after irradiation (Figure 15 B). Nevertheless, there was a significantly reduced baseline mean staining of HIF-1α in the radiosensitive compared to the resistant subgroup (sensitive subgroup: 8.41%, resistant subgroup: 61.82%, *p<0.05*, Figure 15 A). The highest values were found in B339, the 2nd radioresistant cell line in our experiments. There was no change of positive stained cells after irradiation identifiable. The higher amount of HIF-1α positive stained cells in the resistant subgroup is in line with the common literature (refer to 1.2), which identified HIF-1α upregulation as a cause for RT resistance.
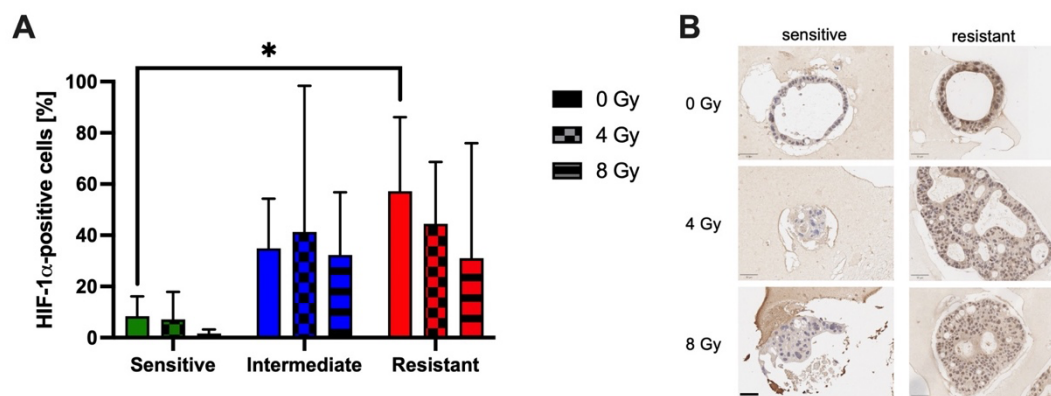
Figure 15: A: Comparison of the mean percentage of HIF-1α positive stained cells of the 3 radiosensitivity subgroups after irradiation with 0 Gy, 4 Gy and 8 Gy. Color scheme and sorting from left to right is according to the above described radiosensitivity classes. There was a significant difference between the mean of the sensitive and the resistant subgroup at 0 Gy (*=p<0.05). Error bars represent SD. **B:** HIF-1α staining 24h after irradiation with 0 Gy, 4 Gy and 8 Gy of representative PDOs from the sensitive and the resistant subgroup. Scale bars equal 50 μm.

4.3. Gene expression signatures associated with radioresistance

The RNA-sequencing data are, except for B211, derived from *in vitro* treatment naive PDOs. All data is collected from one analysis batch. The RNA-sequencing for B169 was performed in a different analysis batch and therefore was excluded from the subclass comparison. For B326 there was no RNA-sequencing data available.

The following subclasses were formed by using the radioresponse data from the CellTiter-Glo® 3D Cell Viability Assay:

Sensitive: B283, B211
Intermediate: B188, B290
Resistant: B320, B339, B226

To understand which pathways are important in the development of radioresistance and maybe crucial for therapeutic approaches, the RNA-data of the subclasses were compared. The various processes showed different regulation between the radioresponse subclasses (Figure 16). A strong signal in upregulation of the hypoxia pathway gene set was detected for the sensitive subclass. The normalized enrichment score (NES, normalized to the size of the

set) comparing the resistant with the sensitive subgroup was *-1.95* (p_{adj} = *0.0001109*) and comparing the intermediate with the sensitive group the NES was *-2.64* (p_{adj} = *3.4 * 10^{-17}*). The negative sign refers to the lower enrichment levels in the opposed subgroups in the hypoxia gene set. Similar results were observed in the *hallmark Epithelial-Mesenchymal-Transition*: Resistant vs. sensitive: NES *-2.06* (p_{adj} = *1.07 * 10^{-5}*), Intermediate vs. sensitive: NES *-2.09* (p_{adj} = *5.78 * 10^{-8}*).
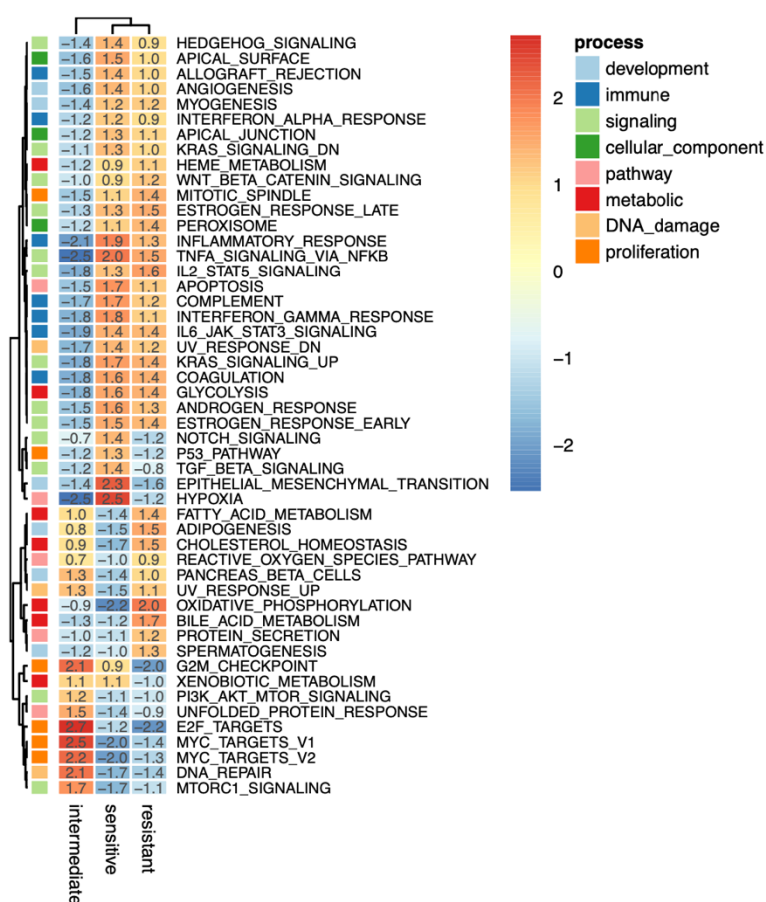

Figure 16: Hallmarks gene sets (Liberzon et al., 2015) with a one-vs-rest comparison of the three radiosensitivity subclasses.

Other interesting findings were detected in the oxidative phosphorylation (OXPHOS) pathway (Figure 17). Radioresistant PDOs showed a higher expression of OXPHOS related genes, which promote an oxygen-dependent

metabolism in the mitochondrial respiration (Reyes-Castellanos, Masoud, & Carrier, 2020), emphasizing the potential for radiosensitization.
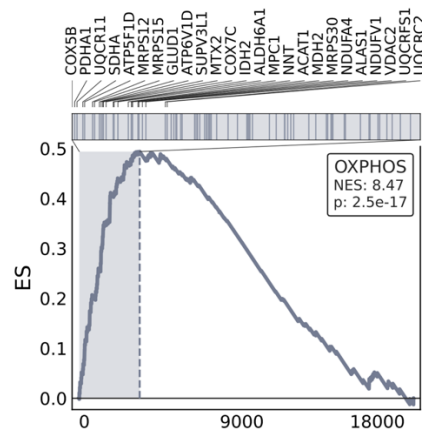

Figure 17: GSEA of the radioresistant subclass. OXPHOS (Hallmark) dependent genes are significantly upregulated (NES 8.57, p<0.0001).

Moffitt et al. (2015) defined a basal and classical subtype based on a large PDAC gene expression study. Figure 18 shows a GSEA with the gene signatures of both subtypes. The resistant subclass showed a strong match with the classical subtype (NES: 6.47, $p_{adj} = 9.5 * 10^{-11}$) and the sensitive subclass with the basal-like subtype (NES: 5.32, $p_{adj} = 1.1 * 10^{-7}$).
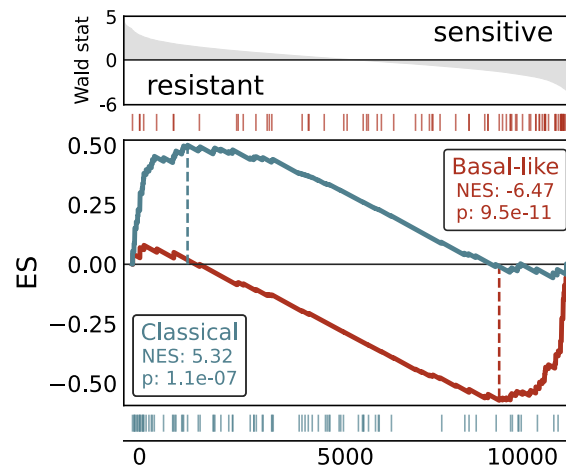

Figure 18: GSEA of resistant and sensitive subclass with Moffitt et. al (2015) classical and basal-like subtype gene set.

4.4. Orthotopic xenograft tumor model

MRI evaluation for PC offers a superior contrast resolution for small non-contour-deforming lesions compared to CT (Miller, Rini, & Keppke, 2006), which makes it particularly valuable for tumor characterization in mice. In the axial slices at the height of the pancreas the kidneys, spinal cord and parts of the gut as well as the stomach are visible. A moderately hyperintense signal alteration occurred in two mice in the region of the pancreas seven weeks after implantation (Figure 19). Nevertheless, there was no clear tumor growth visible in the MR images after 5 months. The above-described MRI lesions did not show a further increase in size or histopathological correlate in further analysis. A repetition of the experiments with doubling of the cell number was performed but did not lead to a measurable unambiguous tumor growth.
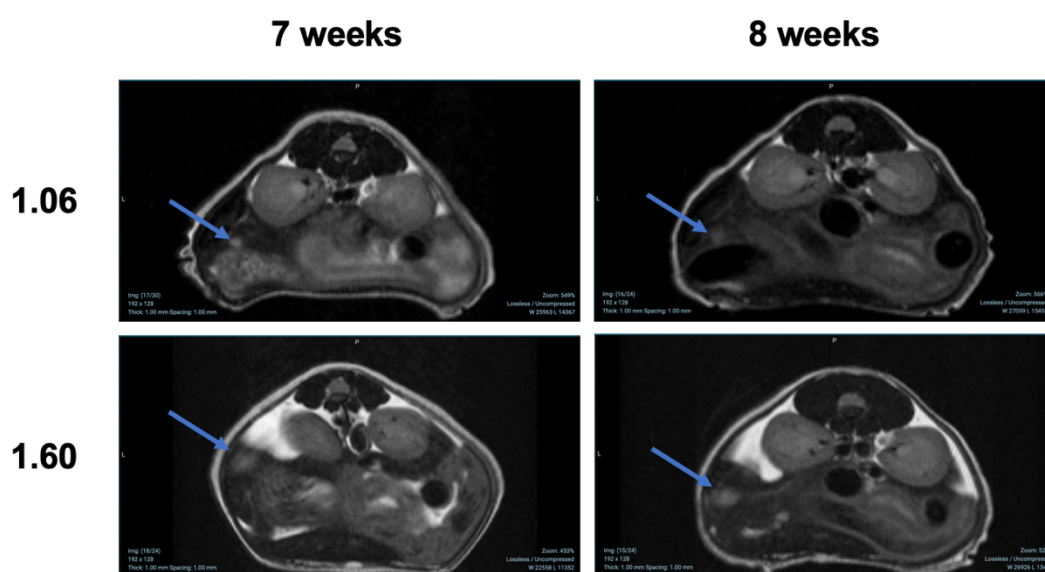
Figure 19: Axial MRI slices of mice with orthotopically implanted PDO B140 seven and eight weeks after implantation of 500.000 cells. Blue arrows point towards hyperintense signal alterations in the anatomical region of the pancreas.

4.5. Correlation with patient data aiming translation

The clinical data from the patient cohort was collected in the hospital information system of the *Klinikum rechts der Isar* and is shown in table 13 and 14. Due to loss in follow-up or incomplete documentation not all information was available at the time of finalization of this thesis. The relative cell viability of the PDOs was

compared with different variables like OS, occurrence of metastasis, tumor stage or the initial serum level of Ca-19.9.

PDO lines B188 and B211 are generated from the same patient. Sampling of the specimen for PDO B188 was done at time point of diagnosis before the administration of 4 cycles FOLFIRINOX regimen and B211 afterwards at time point of surgery. For better visualization, B211 was included in the depicted graphs but excluded from the statistical analysis, to avoid distortion of the calculation. There is no information on the date of death available for the corresponding patients of PDO B320 (radioresistant subgroup). The patients of the PDOs B169, B283 and B326 were in complete remission and presented neither metastasis nor local relapse in the follow-up at the time of the data request (July 2023). Comparing the OS of the three most radiosensitive with the three most resistant PDOs a significant difference was measurable ($p<0.0001$). The three most sensitive PDOs (B283, B326 and B169, as B211 was excluded) showed a mean OS of 40 months while the three most resistant PDOs (B320, B339, B226) had a mean survival of only 2 months (Figure 20). A significant negative correlation, of the radiosensitivity with the OS was visible (Pearson's R: -0.805, $p<0.01$, Figure 21)

There was no correlation with other parameters like age, sex, tumor location, tumor stage, occurrence of metastasis or serum level of tumor markers.
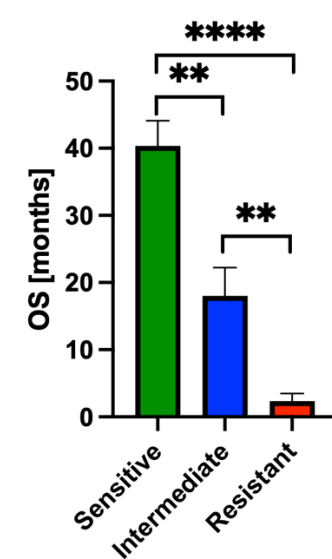
Figure 20: Mean OS of the patients of the corresponding three radioresponse subgroups. Color scheme is according to the before described radiosensitivity classes. (**=$p<0.01$; ****=$p<0.0001$). Error bars represent SD.

Figure 21: Scatter plot and linear regression of relative cell viability at 8 Gy with OS visualizes a significant negative correlation (Pearson's R: -0.805, p<0.01). Color scheme is according to the before described radiosensitivity classes.

5. Discussion

As PDAC remains one of the deadliest diseases, with increasing incidence over the last decades, there is an urgent need for improvement in therapy. Unfortunately, the advances made in the treatment of other types of tumors could not be transferre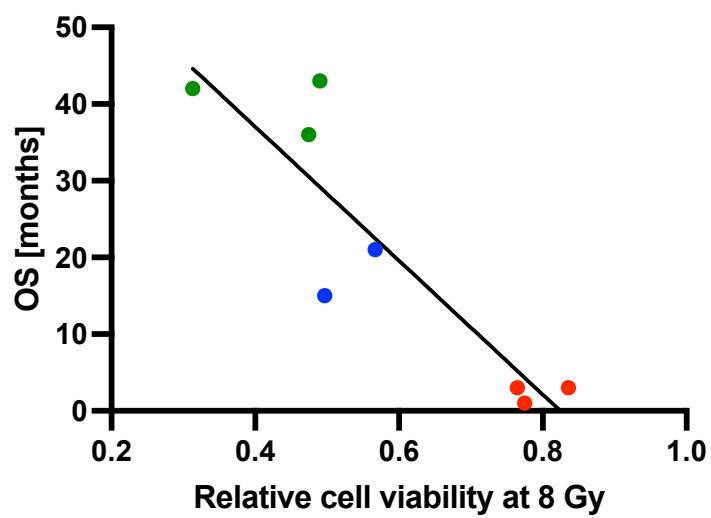d to PC. PDOs offer the opportunity to develop novel therapeutic options and to find the best individual therapy for the patient. The use of PDOs as a research platform has highly increased over the last years. In many tumor entities PDOs have become a solid model for different applications, like drug testing, DNA isolation, microscopic analysis, or generation of xenografts. Especially for the translation from preclinical research to the use in clinical practice, like the adjustment of therapy regiments, PDOs are an excellent tool. It is clear that future therapies must be highly personalized. As our knowledge about the heterogeneity and genetic diversity of cancer grows, we can better understand its consequent inconsistency in response to therapy. PDAC PDOs keep the individual patient's genomic heterogeneity and can be used as a tumor in a shell (Romero-Calvo et al., 2019). Therefore, PDOs hold the capability to test a large number and combination of different therapeutic options as well as to understand the underlying molecular-biological mechanisms. Tiriac et al. (2018) showed in a retrospective study with a large PDO library that the *in vitro* treatment reflects the patient's response to chemotherapy and in combination with DNA- and RNA-sequencing could be used as decision guidance for choosing therapeutics. The goal of this thesis is to test PDOs as a prediction tool for response to RT.

5.1. PDOs as a model for radiation biology

The use of PDOs for the determination of the response to RT is not as well investigated as in chemotherapeutics at this moment. For locally advanced rectal cancer the use as predicting tool for combined RCT was proven with a total number of 80 organoid lines (Yao et al., 2020). In their study not only the cell titer glo assay was used but it could also be shown that the organoid size correlates

with the cell viability. Naumann et al. (2022) demonstrated that the PDO model is also feasible to research the effects of proton and photon therapy in PDAC.

5.1.1. Radioresponse of PDOs reflects clinical heterogeneity

The use of the CellTiter-Glo 3D assay with an ATP dependent luciferase to evaluate the cell viability of 3D organoid structures is broadly applied as gold standard method. Although other techniques like measurements of the organoid diameter exist, we decided to use the CellTiter-Glo assay, since the morphological characteristics of our PDOs differed between the cell lines, for example by cystic or solid formations. Also, apoptotic cell agglomerates cannot be clearly identified with bright field microscopy. Firstly, we used the 72h time point for read out of the cell viability. The experimental setup was optimized since the data with a total of 11 PDOs showed 72 h after irradiation neither a large scatter nor a decrease in cell viability. A further increase of the highest applied dose from 8 Gy to 16 Gy did only reveal a little effect on the decrease of the cell viability. As a next step different time points for performing the cell viability assay were evaluated. The one-week time point showed a distinct decrease in cell viability compared to the 72h time point. In context with the need for fast decision making in clinical application of RT we decided to use the one-week timepoint for further experiments. Naumann et al reported the differences in viability vanished after 13 days compared to six days after irradiation. In our experiments we observed opposite results. However, at the two-week time point we only screened two representatives and not four PDOs, as reported in Naumann et al's publication. In line with our data, the previously mentioned study of Yao et. al did also not show such decrease in the cell viability heterogeneity 15 days after irradiation PDOs. They even observed an increase of the difference in between the organoid area as a surrogate marker for the cell viability after 24 days. The data for the chemotherapeutic agents (5-Fluoruracil and Irinotecan) depicted a similar behavior. Additional to our data, we assume that Yao et. al's findings are transferable to different tumor entities, suggesting that our results supply a reasonable model to reflect the clinically observed heterogeneity in response to RT. Certainly, there is a need for further investigation to understand these differences.

We could show that the response to the irradiation of our cohort of nine PDOs is

highly heterogenous and we were able to identify three different subgroups. radiosensitive, intermediate and radioresistant. To subclassify the groups, we decided to use the cell viability at 8 Gy rather than AUC, because the differences between the PDOs were distinctly less pronounced in the AUC. This heterogeneity gives valuable insight into the differences in the radiobiology of the primary samples. As the organoids retain the genetic identity of the tumor, the results could also be translated to patient therapy. The *in vitro* results were robust and repeatable. This offers the chance to integrate the preclinical screening of the radiosensitivity in the clinical routine for treatment planning. As a timely start of the treatment is of great importance due to the rapid progression of the disease, the methods would have to be automated and standardized as already established in other entities (Choo et al., 2021).

The comparison of the two PDO lines B188 and B211 is of particular note, because these specimens are derived from the same patient before (B188) and after (B211) neoadjuvant treatment with FOLFIRINOX. Our results show an increase in radiosensitivity of B211 compared to B188. This information opens the possibility that RT might be a promising therapeutic option after induction chemotherapy. It also highlights the change in the tumor's genetic expression after chemotherapy, which leads to this change in response to RT. Nevertheless, these results require confirmation by further pairs of such samples.

5.1.2. Radiobiological characterization identifies mechanisms of radioresistance

To gain an understanding of the underlying mechanisms of tumor radioresistance, we performed immunohistochemistry (IHC) on PDOs to analyze DNA damage, proliferation, and hypoxia. Additionally, all slices were stained with hematoxylin and eosin (HE) to identify structural features.

As previously described, staining of γ-H2ax positive cell nuclei allowed us to quantify the extent of DNA double-strand breaks (DSBs). As expected, the DSBs increased following the application of a 4 Gy dose, compared to the control group. Doubling the dose to 8 Gy resulted in almost no further increase in γ-H2ax positive cells. The sensitive subgroup exhibited a significantly higher percentage of positively stained cells after dose application, indicating potentially lower DNA

damage in the more resistant lines. This finding, among others, may account for their higher resistance to radiation.

These results underscore the rationality of utilizing PDOs as a model to study the effects of RT at the cellular level, enabling further characterization and exploration of radioresistance mechanisms.

Ki-67 is a frequently used cellular marker for quantifying the proportion of proliferating cells within a population and is gaining increasing importance in PDAC prognosis due to its correlation with tumor aggressiveness (Pergolini et al., 2019). Moreover, a high Ki-67 proliferation index has been shown to correlate with enhanced susceptibility to RT in other cancer types, such as oral squamous cell carcinoma, (Freudlsperger, Freier, Hoffmann, & Engel, 2012) small cell lung cancer (Ishibashi et al., 2017) and as well with a high complete pathological response after neoadjuvant breast cancer treatment (Wajid, Samad, Syed, & Kazi, 2021).

In line with the aforementioned studies, our cohort's radiosensitive PDO subgroup demonstrated a significantly higher baseline percentage of Ki-67 positive cells (proliferation index). These findings suggest that Ki-67 could potentially serve as a valuable prognostic marker for radiosensitivity in PDAC.

HIF-1α is a well-known transcription factor elevated as a response to hypoxia (Elzakra & Kim, 2021). Elevated HIF-1α is associated with worse prognosis and earlier occurence of metastasis in PDAC (Zoa et al., 2022). Not only the hypoxic microenvironment itself but also the activation of various upstream genes via HIF leads towards radioresistance (Xia, Jiang, & Zhong, 2018). Our results of the IHC staining with HIF-1α show significant lower values in the radiosensitive subgroup matching with these well researched microbiological mechanisms. These findings emphasize the role of HIF-1α as a predicting factor for the success of RT as well as its usage as possible target for radiosensitizing the tumor.

Combining the three markers (DNA double-strand break marker γ-H2ax, proliferation index Ki-67, and hypoxia marker HIF-1α) IHC provides a robust tool for advancing radiobiological characterization and predicting sensitivity to

irradiation. However, the translation of these *in vitro* experiments to patient treatment requires further investigation.

5.2. Identification of predicting pathways for radiosensitivity and potential targets

The sequencing of the transcriptome provides relevant insights into possible mechanisms for radioresistance and subsequently targets for improving radiosensitivity. The rapid availability of the RNA-sequencing data enables rapid decision-making in the clinical environment in the best interest of the patient.

5.2.1. Hypoxia

As described before, PDAC is known to be accompanied with a firm and swollen surrounding tissue, compressing the blood vessels thus creating a hypoxic environment (Kanat & Ertas, 2018, p. 4268). Hypoxia is correlating with an aggressive tumor biology and chemo- as well as radioresistance (Xia et al., 2018). Unexpectedly, the GSEA of hypoxia (*hallmark gene set*, Liberzon et al. (2015), see 4.3) was upregulated in the sensitive subgroup. These counterintuitive results are highly significant and raise the question of their origin and implication on radioresistance in our cohort. PDOs were cultivated under the same normoxic conditions and it can be assumed that the PDOs hold the genomic and transcriptomic consistency of the origin tumor over the time (Romero-Calvo et al., 2019).

The results of our HIF-1α staining, in which the amount of HIF-1α positive cells were significantly higher in the radioresistant subgroup, are contrary to the above described GSEA results. However, looking at HIF-1α at the level of differentially expressed genes (DEGs) between the radioresistant and the radiosensitive subgroup (see 4.3) there is a noticeable but non-significant increase in the radioresistant subgroup. The resistant subgroup shows a Log-2-fold change of 0.58 (equals a change of 1.49, *p > 0.05*). Comparing the 0 Gy baseline results of the HIF-1α staining with the *in vitro* treatment naïve HIF-1α RNA-data, the results tend towards the same direction.

The used hypoxia gene set comprises 200 genes and provides a broader overview of the general hypoxic molecular conditions within cells. In our

investigations, one possible explanation for the upregulation of hypoxia-related genes in the radiosensitive subgroup is the origin of PDOs specimens in a hypoxic microenvironment. Genetically stable PDOs maintain increased production of gene products that counteract the original hypoxic environment. This potentially leads to a higher oxygen delivery in stable *in vitro* conditions compared to other subgroups. Consequently, the increased oxygen availability could render tumor cells more susceptible to radical oxygen species, ultimately sensitizing the hypoxic subpopulation to radiation. However, to fully interpret these results, further research and real-time measurements of oxygen levels in PDOs are essential.

OXPHOS is, besides glycolysis, the main source of ATP and is carried out in the mitochondria by several steps in which oxygen is used as terminal electron acceptor. Recent evidence reveals that numerous cancer entities, despite existing in a hypoxic microenvironment, not only employ the well-known effect of upregulating glycolysis to meet their extensive energy demands (Warburg effect) but also exhibit an upregulation of OXPHOS (Ashton, McKenna, Kunz-Schughart, & Higgins, 2018). Especially the hybrid active phenotype, in which both pathways OXPHOS and glycolysis are upregulated, correlated with highly therapy resistant and metastatic tumors (Jia, Park, Jung, Levine, & Kaipparettu, 2018). Viale et al. (2014) could show that in PDAC mouse models a cell subpopulation, that holds pancreatic CSC characteristics, is resistant to anti-cancer treatment and highly dependent on OXPHOS for survival and can sufficiently be addressed by OXPHOS inhibitors (e.g. oligomycin). The reduction of the oxygen consumption rate via OXPHOS inhibition in hypoxic tumors to reach higher oxygen levels is a promising target to sensitize resistant tumors for radio- as well as chemotherapy, as other strategies to overcome tumor hypoxia have failed in the past (Higgins, O'Cathail, Muschel, & McKenna, 2015). Several already approved drugs originally administered for other purposes as well as only *in vitro* tested substances are available for OXPHOS-inhibition (Ashton et al., 2018). An ongoing phase I trial is already investigating the effects of metformin, a diabetes type II medication and inhibitor of OXPHOS, together with stereotactic RT on the outcome of patients with borderline-resectable or locally-advanced PC (ClinicalTrials.gov Identifier: NCT02153450).

Our results show a significant upregulation in the GSEA for OXPHOS in the radioresistant subgroup. This is in concordance with the above-mentioned growing evidence on the role of the upregulation of mitochondria metabolism in cancer and its impact on therapy failure. The targeting of this pathway might open the opportunity for radiosensitize particularly resistant PDAC by increasing the tumors oxygen levels. PDOs are an excellent platform to further research the effects of OXPHOS inhibitors and raise the opportunity of rapid clinical translation with the off-label use of already approved drugs for patients with preclinical radioresistant PDAC.

5.2.2. Classical and basal-like subtype

Moffitt et al. (2015) defined a "classical" and a "basal-like" PDAC subtype based on tumors gene expression microarray data. In their study the classical subtype was associated with a distinctly better median OS (classical: 19 months, basal-like: 11 months). Results from the COMPASS-trial showed that patients with the "classical" subtype responded better to first-line chemotherapy with mFOLFIRINOX than patients with the "basal-like" subtype (Aung et al., 2018).

Our results show a strongly pronounced differentiation between Moffitt's "classical" and a "basal-like" subtype in our radioresponse subgroups. The radiosensitive subgroup had a "basal-like" and the radioresistant a "classical" RNA-signature in the GSEA. Regarding the results from the COMPASS-trial this might open the possibility to add RT to the treatment of these aggressive chemo-resistant tumors. The "basal-like" subtype is also described to be accompanied by an upregulation of hypoxia related pathways, as the same was observed in our radiosensitive subgroup.

5.3. Critical consideration of the in vivo model

Our *in vivo* model could not show sufficient growth of pancreatic tumors. Though there was a signal alteration in the MRI T2 sequence in the anatomical pancreatic region after about two months, we did not observe any signs for further tumor growth beyond this point. The general condition of the mice remained stable until an age-related deterioration began. Postmortem histological analysis revealed no clear evidence for PDAC in the analyzed mice. A repetition of the experiments

with a doubling of the implanted number of cells also did not show any success either. A possible reason for this could be that the PDO B140, was despite its fast *in vitro* growth, not suitable for the *in vivo* implantation, perhaps due to the different TME. In previous studies, the tumor take rates for PDAC PDOs have shown considerable variability, ranging from 100% to 0%, depending on the specific PDO line used (Naumann et al., 2022). A repetition with different PDO lines could be rational as the used protocols are validated by other working groups and the technique of the orthotopic PDAC model is well established in our lab (Dobiasch et al., 2021).

5.4. Radiosensitivity subgroups correlate with clinical data

Since B188 and B211 were derived from the same patient, the neoadjuvant treated B211 was excluded from the analysis. The correlation analysis of the PDOs with the OS of the corresponding patients revealed a clear trend towards higher OS in radiosensitive PDOs. The other tested parameters like age, sex, initial serum level of the tumor markers Ca 19-9 and CEA or tumor stage, did not show any correlation with the preclinical radioresponse. Although the data set was rather small, there was a significantly higher OS in the radiosensitive compared to the radioresistant subgroup. The test for *in vitro* radiosensitivity could therefore be useful to estimate the prognosis. Of course, a correlation with the patients' clinical response to RT is needed to further evaluate the reliability of real translation.

5.5. Limitations

Despite the several advantages that PDOs hold for *in vitro* experiments, there are limitations to the methods and results of this thesis. First, the limited sample size of nine specimens makes it difficult to generate significant results. The effects in the subgroups must be strongly pronounced so that the differences are statistically relevant. A continuation of including more PDOs therefore is necessary to validate our current data and to statistically confirm observed trends, which were not significant, as well as to identify new parameters, that influence radioresistance.

Another limiting factor is the absence of stromal components in the TME of the PDOs. As described before, the TME is known to have a major impact on promoting the tumors' therapy resistance, self-renewal capabilities and Epithelial-Mesenchymal-Transition (Schuth et al., 2022). New methods incorporating an organoid-fibroblast co-culture system are available and should be used in follow-up experiments to further investigate the role of the TME on radioresistance.

The specimens in our data set have been gathered from tumors in different stages and from treatment-naïve patients as well as patients after chemotherapy. Tumor cells tend to change their biology towards more aggressiveness and resistance after being exposed to chemo treatments. This heterogeneous initial tumor stage of the PDOs makes it difficult to project the results regarding cell viability after irradiation to a possible resistance to RT in the patient.

PDAC is known to feature an intra-tumoral heterogeneity on transcriptional level depending on the area the sample was taken (Liu et al., 2022). As PDOs are derived from mostly only one location in the tumor this also limits the interpretability of the results of the *in vitro* testing for a prognosis of RT.

Limitations also arise from a technical angle. The success of generating PDOs from fine-needle aspiration or surgical specimens varies. Also, the often-slow *in vitro* growth prolongs the time until enough material is collected to perform the experiments and subsequently create the output for the therapy recommendation. Automated and standardized approaches of seeding, treatment and evaluation promise a solution to a part of the problem because less tumor material is required.

6. Summary and Outlook

PDAC remains one of the cancer entities with the worst clinical outcome despite the several years and highest efforts, that were put into the research to overcome treatment resistances. Even though our knowledge on individual tumor biology, the role of the TME or CSC has grown rapidly over the last years this output could unfortunately not be translated into longer OS. Therefore, new research models to identify treatment options are desperately needed. In Germany, RT is not broadly used in our toolbox against PC and clinical trials with combined RCT provided heterogenic results emphasizing the need for personalized therapy (Dobiasch et al., 2018). Important steps on the way to a sustainable therapy for PC are the identification of predicting biomarkers, which help us to early identify patients with radiosensitive tumors and, moreover, discover targetable mechanisms for radioresistance.

The recent development of PDOs as a novel research platform has given us an opportunity to accomplish these steps. We can use PDOs to realize highly individualized therapies by rapidly providing results from the *in vitro* characterization for the decision-making process.

We showed that PDAC PDOs could reflect the heterogeneity in response to irradiation by measuring the cell viability of nine different PDO lines and it was possible to identify a radiosensitive, an intermediate and a radioresistant subgroup.

By IHC staining we discovered possible markers for radiosensitivity like significantly higher grades of γ-H2ax and KI-67 positive cells as well as lower levels of HIF-1α.
Furthermore, the analysis of the RNA-sequencing data revealed promising results. The highly significant upregulation of OXPHOS related pathways in the resistant subgroup, which is consistent with current research, provides the possibility of radiosensitization by using one of the various inhibitors available.

Of particular note is that the OS was significantly higher in the radiosensitive compared to the in translational research.

All of these results underline the use of PDOs as a precious tool for individualized RT of PC patients. Further research is essential to deepen our knowledge of the above-mentioned mechanisms and especially to provide a real translation into the clinic.

Reference list

Abrams, R. A., Winter, K. A., Safran, H., Goodman, K. A., Regine, W. F., Berger, A. C., . . . Crane, C. H. (2020). Results of the NRG Oncology/RTOG 0848 Adjuvant Chemotherapy Question-Erlotinib+Gemcitabine for Resected Cancer of the Pancreatic Head: A Phase II Randomized Clinical Trial. *Am J Clin Oncol, 43*(3), 173-179. doi:10.1097/coc.0000000000000633

Alvarez, M. J., Shen, Y., Giorgi, F. M., Lachmann, A., Ding, B. B., Ye, B. H., & Califano, A. (2016). Functional characterization of somatic mutations in cancer using network-based inference of protein activity. *Nat Genet, 48*(8), 838-847. doi:10.1038/ng.3593

Ashton, T. M., McKenna, W. G., Kunz-Schughart, L. A., & Higgins, G. S. (2018). Oxidative Phosphorylation as an Emerging Target in Cancer Therapy. *Clin Cancer Res, 24*(11), 2482-2490. doi:10.1158/1078-0432.Ccr-17-3070

Aung, K. L., Fischer, S. E., Denroche, R. E., Jang, G. H., Dodd, A., Creighton, S., . . . Knox, J. J. (2018). Genomics-Driven Precision Medicine for Advanced Pancreatic Cancer: Early Results from the COMPASS Trial. *Clin Cancer Res, 24*(6), 1344-1354. doi:10.1158/1078-0432.Ccr-17-2994

Bach, M. L., D. (2019). Verifying Cell-Based Assays for Use with 3D Models. *Promega Corporation*. Retrieved from https://www.promega.de/resources/pubhub/2019/verifying-cell-based-assays-for-use-with-3d-models/

Baker, L. A., Tiriac, H., & Tuveson, D. A. (2019). Generation and Culture of Human Pancreatic Ductal Adenocarcinoma Organoids from Resected Tumor Specimens. *Methods Mol Biol, 1882*, 97-115. doi:10.1007/978-1-4939-8879-2_9

Bankhead, P., Loughrey, M. B., Fernández, J. A., Dombrowski, Y., McArt, D. G., Dunne, P. D., . . . Hamilton, P. W. (2017). QuPath: Open source software for digital pathology image analysis. *Sci Rep, 7*(1), 16878. doi:10.1038/s41598-017-17204-5

Behrens, G., Jochem, C., Schmid, D., Keimling, M., Ricci, C., & Leitzmann, M. F. (2015). Physical activity and risk of pancreatic cancer: a systematic review and meta-analysis. *Eur J Epidemiol, 30*(4), 279-298. doi:10.1007/s10654-015-0014-9

Bosetti, C., Bravi, F., Turati, F., Edefonti, V., Polesel, J., Decarli, A., . . . Zeegers, M. P. (2013). Nutrient-based dietary patterns and pancreatic cancer risk. *Ann Epidemiol, 23*(3), 124-128. doi:10.1016/j.annepidem.2012.12.005

Bosetti, C., Lucenteforte, E., Silverman, D. T., Petersen, G., Bracci, P. M., Ji, B. T., . . . La Vecchia, C. (2012). Cigarette smoking and pancreatic cancer: an analysis from the International Pancreatic Cancer Case-Control Consortium (Panc4). *Ann Oncol, 23*(7), 1880-1888. doi:10.1093/annonc/mdr541

Bosetti, C., Rosato, V., Li, D., Silverman, D., Petersen, G. M., Bracci, P. M., . . . La Vecchia, C. (2014). Diabetes, antidiabetic medications, and pancreatic cancer risk: an analysis from the International Pancreatic Cancer Case-Control Consortium. *Ann Oncol, 25*(10), 2065-2072. doi:10.1093/annonc/mdu276

Bray, F., Ferlay, J., Soerjomataram, I., Siegel, R. L., Torre, L. A., & Jemal, A. (2018). Global cancer statistics 2018: GLOBOCAN estimates of incidence and mortality worldwide for 36 cancers in 185 countries. *68*(6), 394-424. doi:doi:10.3322/caac.21492

Broutier, L., Andersson-Rolf, A., Hindley, C. J., Boj, S. F., Clevers, H., Koo, B. K., & Huch, M. (2016). Culture and establishment of self-renewing human and mouse adult liver and pancreas 3D organoids and their genetic manipulation. *Nat Protoc, 11*(9), 1724-1743. doi:10.1038/nprot.2016.097

Bynigeri, R. R., Jakkampudi, A., Jangala, R., Subramanyam, C., Sasikala, M., Rao, G. V., . . . Talukdar, R. (2017). Pancreatic stellate cell: Pandora's box for pancreatic disease biology. *World J Gastroenterol, 23*(3), 382-405. doi:10.3748/wjg.v23.i3.382

Cadacio, F. N. (2021). *Characterization of the radiation response and the migratory and invasive potential in pancreatic cancer.* (M.Sc. Radiation Biology Master Thesis). Technischen Universität München,

Choo, N., Ramm, S., Luu, J., Winter, J. M., Selth, L. A., Dwyer, A. R., . . . Simpson, K. J. (2021). High-Throughput Imaging Assay for Drug Screening of 3D Prostate Cancer Organoids. *SLAS Discov, 26*(9), 1107-1124. doi:10.1177/24725552211020668

Combs, S. E. (2015). Individualized radiotherapy (iRT) concepts for locally advanced pancreatic cancer (LAPC): indications and prognostic factors. *Langenbeck's Archives of Surgery, 400*(7), 749-756. doi:10.1007/s00423-015-1309-8

Conroy, T., Castan, F., Lopez, A., Turpin, A., Ben Abdelghani, M., Wei, A. C., . . . Hammel, P. (2022). Five-Year Outcomes of FOLFIRINOX vs Gemcitabine as Adjuvant Therapy for Pancreatic Cancer: A Randomized Clinical Trial. *JAMA Oncol, 8*(11), 1571-1578. doi:10.1001/jamaoncol.2022.3829

Cowley, M. J., Chang, D. K., Pajic, M., Johns, A. L., Waddell, N., Grimmond, S. M., & Biankin, A. V. (2013). Understanding pancreatic cancer genomes. *J Hepatobiliary Pancreat Sci, 20*(6), 549-556. doi:10.1007/s00534-013-0610-6

Dantes, Z., Yen, H. Y., Pfarr, N., Winter, C., Steiger, K., Muckenhuber, A., . . . Reichert, M. (2020). Implementing cell-free DNA of pancreatic cancer patient-derived organoids for personalized oncology. *JCI Insight, 5*(15). doi:10.1172/jci.insight.137809

Destatis, S. B. (2022). Sterbefälle durch Krebs insgesamt 2021. Retrieved from https://www.destatis.de/DE/Themen/Gesellschaft-Umwelt/Gesundheit/Todesursachen/Tabellen/sterbefaelle-krebs-insgesamt.html

Deutsche Krebsgesellschaft, D. K., AWMF. (2013). *S3-Leitlinie Exokrines Pankreaskarzinom* [Langversion 1.0, 2013]. In D. K. Leitlinienprogramm Onkologie (Deutsche Krebsgesellschaft, AWMF) (Ed.), ***AWMF Registernummer: 032-010OL***. Retrieved from http://leitlinienprogramm-onkologie.de/Leitlinien.7.0.html

Dobiasch, S., Goerig, N. L., Fietkau, R., & Combs, S. E. (2018). Essential role of radiation therapy for the treatment of pancreatic cancer : Novel study concepts and established treatment recommendations. *Strahlenther Onkol, 194*(3), 185-195. doi:10.1007/s00066-017-1227-5

Dobiasch, S., Kampfer, S., Steiger, K., Schilling, D., Fischer, J. C., Schmid, T. E., . . . Combs, S. E. (2021). Histopathological Tumor and Normal Tissue Responses after 3D-Planned Arc Radiotherapy in an Orthotopic Xenograft Mouse Model of Human Pancreatic Cancer. *Cancers (Basel), 13*(22). doi:10.3390/cancers13225656

Doi, R., Imamura, M., Hosotani, R., Imaizumi, T., Hatori, T., Takasaki, K., . . . Yoshida, S. (2008). Surgery versus radiochemotherapy for resectable locally invasive pancreatic cancer: final results of a randomized multi-institutional trial. *Surg Today, 38*(11), 1021-1028. doi:10.1007/s00595-007-3745-8

Dunne, R. F., & Hezel, A. F. (2015). Genetics and Biology of Pancreatic Ductal Adenocarcinoma. *Hematol Oncol Clin North Am, 29*(4), 595-608. doi:10.1016/j.hoc.2015.04.003

Elzakra, N., & Kim, Y. (2021). HIF-1α Metabolic Pathways in Human Cancer. *Adv Exp Med Biol, 1280*, 243-260. doi:10.1007/978-3-030-51652-9_17

Ene-Obong, A., Clear, A. J., Watt, J., Wang, J., Fatah, R., Riches, J. C., . . . Kocher, H. M. (2013). Activated pancreatic stellate cells sequester CD8+ T cells to reduce their infiltration of the juxtatumoral compartment of pancreatic ductal adenocarcinoma. *Gastroenterology, 145*(5), 1121-1132. doi:10.1053/j.gastro.2013.07.025

Eser, S., Schnieke, A., Schneider, G., & Saur, D. (2014). Oncogenic KRAS signalling in pancreatic cancer. *Br J Cancer, 111*(5), 817-822. doi:10.1038/bjc.2014.215

Fatima, Z., Alhabhbeh, A., Darweesh, M., Laswi, H., & Manthri, S. (2022). A systemic review and meta-analysis of FOLFIRINOX vs gemcitabine plus nab-paclitaxel in the neoadjuvant treatment of localized pancreatic cancer. *Journal of Clinical Oncology, 40*(16_suppl), e16272-e16272. doi:10.1200/JCO.2022.40.16_suppl.e16272

Feig, C., Gopinathan, A., Neesse, A., Chan, D. S., Cook, N., & Tuveson, D. A. (2012). The pancreas cancer microenvironment. *Clin Cancer Res, 18*(16), 4266-4276. doi:10.1158/1078-0432.Ccr-11-3114

Ferlay, J., Ervik, M., Lam, F., Colombet, M., Mery, L., Piñeros, M., . . . Bray, F. (2018). Global Cancer Observatory: Cancer Today. Lyon, France: International Agency for Research on Cancer. Available from: https://gco.iarc.fr/today, accessed 28 Ferbruary 2019.

Fietkau, R., Ghadimi, M., Grützmann, R., Wittel, U. A., Jacobasch, L., Uhl, W., . . . Oettle, H. (2022). Randomized phase III trial of induction chemotherapy followed by chemoradiotherapy or chemotherapy alone for nonresectable locally advanced pancreatic cancer: First results of the CONKO-007 trial. *Journal of Clinical Oncology, 40*(16_suppl), 4008-4008. doi:10.1200/JCO.2022.40.16_suppl.4008

Forsmark, C. E., Lambiase, L., & Vogel, S. B. (1994). Diagnosis of pancreatic cancer and prediction of unresectability using the tumor-associated antigen CA19-9. *Pancreas, 9*(6), 731-734. doi:10.1097/00006676-199411000-00010

Frappart, P. O., & Hofmann, T. G. (2020). Pancreatic Ductal Adenocarcinoma (PDAC) Organoids: The Shining Light at the End of the Tunnel for Drug Response Prediction and Personalized Medicine. *Cancers (Basel), 12*(10). doi:10.3390/cancers12102750

Freudlsperger, C., Freier, K., Hoffmann, J., & Engel, M. (2012). Ki-67 expression predicts radiosensitivity in oral squamous cell carcinoma. *Int J Oral Maxillofac Surg, 41*(8), 965-969. doi:10.1016/j.ijom.2012.04.014

Gerdes, J., Lemke, H., Baisch, H., Wacker, H. H., Schwab, U., & Stein, H. (1984). Cell cycle analysis of a cell proliferation-associated human nuclear antigen defined by the monoclonal antibody Ki-67. *J Immunol, 133*(4), 1710-1715.

Gillen, S., Schuster, T., Meyer Zum Büschenfelde, C., Friess, H., & Kleeff, J. (2010). Preoperative/neoadjuvant therapy in pancreatic cancer: a systematic review and meta-analysis of response and resection percentages. *PLoS Med, 7*(4), e1000267. doi:10.1371/journal.pmed.1000267

Hamada, S., Masamune, A., Takikawa, T., Suzuki, N., Kikuta, K., Hirota, M., . . . Shimosegawa, T. (2012). Pancreatic stellate cells enhance stem cell-like phenotypes in pancreatic cancer cells. *Biochem Biophys Res Commun, 421*(2), 349-354. doi:10.1016/j.bbrc.2012.04.014

Higgins, G. S., O'Cathail, S. M., Muschel, R. J., & McKenna, W. G. (2015). Drug radiotherapy combinations: review of previous failures and reasons for future optimism. *Cancer Treat Rev, 41*(2), 105-113. doi:10.1016/j.ctrv.2014.12.012

Hruban, R. H., Goggins, M., Parsons, J., & Kern, S. E. (2000). Progression model for pancreatic cancer. *Clin Cancer Res, 6*(8), 2969-2972.

Ishibashi, N., Maebayashi, T., Aizawa, T., Sakaguchi, M., Nishimaki, H., & Masuda, S. (2017). Correlation between the Ki-67 proliferation index and response to radiation therapy in small cell lung cancer. *Radiation Oncology, 12*(1), 16. doi:10.1186/s13014-016-0744-1

Jones, S., Zhang, X., Parsons, D. W., Lin, J. C., Leary, R. J., Angenendt, P., . . . Kinzler, K. W. (2008). Core signaling pathways in human pancreatic cancers revealed by global genomic analyses. *Science, 321*(5897), 1801-1806. doi:10.1126/science.1164368

Kanat, O., & Ertas, H. (2018). Shattering the castle walls: Anti-stromal therapy for pancreatic cancer. *World J Gastrointest Oncol, 10*(8), 202-210. doi:10.4251/wjgo.v10.i8.202

Kapałczyńska, M., Kolenda, T., Przybyła, W., Zajączkowska, M., Teresiak, A., Filas, V., . . . Lamperska, K. (2018). 2D and 3D cell cultures - a comparison of different types of cancer cell cultures. *Arch Med Sci, 14*(4), 910-919. doi:10.5114/aoms.2016.63743

Kasper, D. L., Fauci, A. S., Hauser, S. L., Longo, D. L., Jameson, J. L., Loscalzo, J., . . . Harrison, T. R. (2016). *Harrisons Innere Medizin* (19. Auflage, deutsche Ausgabe ed.). New York: McGraw-Hill Education.

Katz, M. H. G., Shi, Q., Meyers, J., Herman, J. M., Chuong, M., Wolpin, B. M., . . . O'Reilly, E. M. (2022). Efficacy of Preoperative mFOLFIRINOX vs mFOLFIRINOX Plus Hypofractionated Radiotherapy for Borderline Resectable Adenocarcinoma of the Pancreas: The A021501 Phase 2 Randomized Clinical Trial. *JAMA Oncol, 8*(9), 1263-1270. doi:10.1001/jamaoncol.2022.2319

Kirkegard, J., Mortensen, F. V., & Cronin-Fenton, D. (2017). Chronic Pancreatitis and Pancreatic Cancer Risk: A Systematic Review and Meta-analysis. *Am J Gastroenterol, 112*(9), 1366-1372. doi:10.1038/ajg.2017.218

Kolde, R. (2019). Pretty Heatmaps. Retrieved from https://cran.r-project.org/package=pheatmap

Kopp, J. L., von Figura, G., Mayes, E., Liu, F. F., Dubois, C. L., Morris, J. P. t., . . . Sander, M. (2012). Identification of Sox9-dependent acinar-to-ductal reprogramming as the principal mechanism for initiation of pancreatic ductal adenocarcinoma. *Cancer Cell, 22*(6), 737-750. doi:10.1016/j.ccr.2012.10.025

Korotkevich, G., Sukhov, V., Budin, N., Shpak, B., Artyomov, M. N., & Sergushichev, A. (2021). Fast gene set enrichment analysis. *bioRxiv*, 060012. doi:10.1101/060012

Lancaster, M. A., & Huch, M. (2019). Disease modelling in human organoids. *Dis Model Mech, 12*(7). doi:10.1242/dmm.039347

Larsson, S. C., & Wolk, A. (2012). Red and processed meat consumption and risk of pancreatic cancer: meta-analysis of prospective studies. *Br J Cancer, 106*(3), 603-607. doi:10.1038/bjc.2011.585

Liberzon, A., Birger, C., Thorvaldsdóttir, H., Ghandi, M., Mesirov, J. P., & Tamayo, P. (2015). The Molecular Signatures Database (MSigDB) hallmark gene set collection. *Cell Syst, 1*(6), 417-425. doi:10.1016/j.cels.2015.12.004

Liu, X., Wang, W., Liu, X., Zhang, Z., Yu, L., Li, R., . . . Liang, Z. (2022). Multi-omics analysis of intra-tumoural and inter-tumoural heterogeneity in pancreatic ductal adenocarcinoma. *Clin Transl Med, 12*(1), e670. doi:10.1002/ctm2.670

Lonza. (2012). MycoAlertTM Assay Control Set Instructions for Use. *Lonza Walkersville, Inc.* Retrieved from https://bioscience.lonza.com/lonza_bs/DE/en/download/product/asset/27672

Love, M. I., Huber, W., & Anders, S. (2014). Moderated estimation of fold change and dispersion for RNA-seq data with DESeq2. *Genome Biol, 15*(12), 550. doi:10.1186/s13059-014-0550-8

McWilliams, R. R., Rabe, K. G., Olswold, C., De Andrade, M., & Petersen, G. M. (2005). Risk of malignancy in first-degree relatives of patients with pancreatic carcinoma. *Cancer, 104*(2), 388-394. doi:10.1002/cncr.21166

Miller, F. H., Rini, N. J., & Keppke, A. L. (2006). MRI of adenocarcinoma of the pancreas. *AJR Am J Roentgenol, 187*(4), W365-374. doi:10.2214/ajr.05.0875

Moffitt, R. A., Marayati, R., Flate, E. L., Volmar, K. E., Loeza, S. G., Hoadley, K. A., . . . Yeh, J. J. (2015). Virtual microdissection identifies distinct tumor- and stroma-specific subtypes of pancreatic ductal adenocarcinoma. *Nat Genet, 47*(10), 1168-1178. doi:10.1038/ng.3398

Moreira, L., Bakir, B., Chatterji, P., Dantes, Z., Reichert, M., & Rustgi, A. K. (2018). Pancreas 3D Organoids: Current and Future Aspects as a Research Platform for Personalized Medicine in Pancreatic Cancer. *Cell Mol Gastroenterol Hepatol, 5*(3), 289-298. doi:10.1016/j.jcmgh.2017.12.004

Morris, J. P. t., Wang, S. C., & Hebrok, M. (2010). KRAS, Hedgehog, Wnt and the twisted developmental biology of pancreatic ductal adenocarcinoma. *Nat Rev Cancer, 10*(10), 683-695. doi:10.1038/nrc2899

Mueller, S., Engleitner, T., Maresch, R., Zukowska, M., Lange, S., Kaltenbacher, T., . . . Rad, R. (2018). Evolutionary routes and KRAS dosage define pancreatic cancer phenotypes. *Nature, 554*(7690), 62-68. doi:10.1038/nature25459

Nagle, P. W., Plukker, J. T. M., Muijs, C. T., van Luijk, P., & Coppes, R. P. (2018). Patient-derived tumor organoids for prediction of cancer treatment response. *Semin Cancer Biol, 53*, 258-264. doi:10.1016/j.semcancer.2018.06.005

Naudin, S., Li, K., Jaouen, T., Assi, N., Kyro, C., Tjonneland, A., . . . Ferrari, P. (2018). Lifetime and baseline alcohol intakes and risk of pancreatic cancer in the European Prospective Investigation into Cancer and Nutrition study. *Int J Cancer, 143*(4), 801-812. doi:10.1002/ijc.31367

Naumann, M., Czempiel, T., Lößner, A. J., Pape, K., Beyreuther, E., Löck, S., . . . Dietrich, A. (2022). Combined Systemic Drug Treatment with Proton Therapy: Investigations on Patient-Derived Organoids. *Cancers (Basel), 14*(15). doi:10.3390/cancers14153781

NCCN. (2020). Pancreatic Adenocarcinoma (Version 1.2020). Retrieved from https://www.nccn.org/professionals/physician_gls/pdf/pancreatic_blocks.pdf

Neoptolemos, J. P., Stocken, D. D., Bassi, C., Ghaneh, P., Cunningham, D., Goldstein, D., . . . Büchler, M. W. (2010). Adjuvant chemotherapy with fluorouracil plus folinic acid vs gemcitabine following pancreatic cancer resection: a randomized controlled trial. *Jama, 304*(10), 1073-1081. doi:10.1001/jama.2010.1275

Olive, P. L., & Durand, R. E. (1994). Drug and radiation resistance in spheroids: cell contact and kinetics. *Cancer Metastasis Rev, 13*(2), 121-138. doi:10.1007/bf00689632

Park, W., Chawla, A., & O'Reilly, E. M. (2021). Pancreatic Cancer: A Review. *Jama, 326*(9), 851-862. doi:10.1001/jama.2021.13027

Pergolini, I., Crippa, S., Pagnanelli, M., Belfiori, G., Pucci, A., Partelli, S., . . . Falconi, M. (2019). Prognostic impact of Ki-67 proliferative index in resectable pancreatic ductal adenocarcinoma. *BJS Open, 3*(5), 646-655. doi:10.1002/bjs5.50175

Petersen, G. M. (2016). Familial pancreatic cancer. *Seminars in oncology, 43*(5), 548-553. doi:10.1053/j.seminoncol.2016.09.002

Promega. (2015). CellTiter-Glo® 3D Cell Viability Assay technical manual. Retrieved from https://www.promega.de/-/media/files/resources/protocols/technical-manuals/101/celltiter-glo-3d-cell-viability-assay-protocol.pdf?rev=88083aa3f7284e898ff0f218aa3c6b59&sc_lang=en

Pylayeva-Gupta, Y., Grabocka, E., & Bar-Sagi, D. (2011). RAS oncogenes: weaving a tumorigenic web. *Nat Rev Cancer, 11*(11), 761-774. doi:10.1038/nrc3106

Reyes-Castellanos, G., Masoud, R., & Carrier, A. (2020). Mitochondrial Metabolism in PDAC: From Better Knowledge to New Targeting Strategies. *Biomedicines, 8*(8). doi:10.3390/biomedicines8080270

Ritts, R. E., Jr., Nagorney, D. M., Jacobsen, D. J., Talbot, R. W., & Zurawski, V. R., Jr. (1994). Comparison of preoperative serum CA19-9 levels with results of diagnostic imaging modalities in patients undergoing laparotomy for suspected pancreatic or gallbladder disease. *Pancreas, 9*(6), 707-716. doi:10.1097/00006676-199411000-00006

Riva, G., Pea, A., Pilati, C., Fiadone, G., Lawlor, R. T., Scarpa, A., & Luchini, C. (2018). Histo-molecular oncogenesis of pancreatic cancer: From

precancerous lesions to invasive ductal adenocarcinoma. *World J Gastrointest Oncol, 10*(10), 317-327. doi:10.4251/wjgo.v10.i10.317

Rogakou, E. P., Pilch, D. R., Orr, A. H., Ivanova, V. S., & Bonner, W. M. (1998). DNA double-stranded breaks induce histone H2AX phosphorylation on serine 139. *J Biol Chem, 273*(10), 5858-5868. doi:10.1074/jbc.273.10.5858

Romero-Calvo, I., Weber, C. R., Ray, M., Brown, M., Kirby, K., Nandi, R. K., . . . White, K. P. (2019). Human Organoids Share Structural and Genetic Features with Primary Pancreatic Adenocarcinoma Tumors. *Mol Cancer Res, 17*(1), 70-83. doi:10.1158/1541-7786.Mcr-18-0531

Sato, T., Vries, R. G., Snippert, H. J., van de Wetering, M., Barker, N., Stange, D. E., . . . Clevers, H. (2009). Single Lgr5 stem cells build crypt-villus structures in vitro without a mesenchymal niche. *Nature, 459*(7244), 262-265. doi:10.1038/nature07935

Schuth, S., Le Blanc, S., Krieger, T. G., Jabs, J., Schenk, M., Giese, N. A., . . . Strobel, O. (2022). Patient-specific modeling of stroma-mediated chemoresistance of pancreatic cancer using a three-dimensional organoid-fibroblast co-culture system. *J Exp Clin Cancer Res, 41*(1), 312. doi:10.1186/s13046-022-02519-7

Seshacharyulu, P., Baine, M. J., Souchek, J. J., Menning, M., Kaur, S., Yan, Y., . . . Batra, S. K. (2017). Biological determinants of radioresistance and their remediation in pancreatic cancer. *Biochimica et biophysica acta. Reviews on cancer, 1868*(1), 69-92. doi:10.1016/j.bbcan.2017.02.003

Stewart, B. W., & Wild, C. P. (Eds.). (2014). *World Cancer Report 2014*. Lyon: International Agency for Research on Cancer.

Stocken, D. D., Büchler, M. W., Dervenis, C., Bassi, C., Jeekel, H., Klinkenbijl, J. H., . . . Neoptolemos, J. P. (2005). Meta-analysis of randomised adjuvant therapy trials for pancreatic cancer. *Br J Cancer, 92*(8), 1372-1381. doi:10.1038/sj.bjc.6602513

Subramanian, A., Tamayo, P., Mootha, V. K., Mukherjee, S., Ebert, B. L., Gillette, M. A., . . . Mesirov, J. P. (2005). Gene set enrichment analysis: a knowledge-based approach for interpreting genome-wide expression profiles. *Proc Natl Acad Sci U S A, 102*(43), 15545-15550. doi:10.1073/pnas.0506580102

Tang, D., Gao, J., Wang, S., Yuan, Z., Ye, N., Chong, Y., . . . Jiang, K. (2015). Apoptosis and anergy of T cell induced by pancreatic stellate cells-derived galectin-1 in pancreatic cancer. *Tumour Biol, 36*(7), 5617-5626. doi:10.1007/s13277-015-3233-5

Tiriac, H., Belleau, P., Engle, D. D., Plenker, D., Deschênes, A., Somerville, T. D. D., . . . Tuveson, D. A. (2018). Organoid Profiling Identifies Common Responders to Chemotherapy in Pancreatic Cancer. *Cancer Discov, 8*(9), 1112-1129. doi:10.1158/2159-8290.Cd-18-0349

UICC (Ed.) (2017). *TNM classification of malignant tumours 8th E* (Eighth edition ed.). Chichester, West Sussex, UK ; Hoboken, NJ: John Wiley & Sons, Inc.

Valle, S., Martin-Hijano, L., Alcalá, S., Alonso-Nocelo, M., & Sainz, B., Jr. (2018). The Ever-Evolving Concept of the Cancer Stem Cell in Pancreatic Cancer. *Cancers (Basel), 10*(2). doi:10.3390/cancers10020033

Vaziri-Gohar, A., Zarei, M., Brody, J. R., & Winter, J. M. (2018). Metabolic Dependencies in Pancreatic Cancer. *Front Oncol, 8*, 617. doi:10.3389/fonc.2018.00617

Versteijne, E., van Dam, J. L., Suker, M., Janssen, Q. P., Groothuis, K., Akkermans-Vogelaar, J. M., . . . van Eijck, C. H. J. (2022). Neoadjuvant Chemoradiotherapy Versus Upfront Surgery for Resectable and Borderline Resectable Pancreatic Cancer: Long-Term Results of the Dutch Randomized PREOPANC Trial. *J Clin Oncol, 40*(11), 1220-1230. doi:10.1200/jco.21.02233

Viale, A., Pettazzoni, P., Lyssiotis, C. A., Ying, H., Sánchez, N., Marchesini, M., . . . Draetta, G. F. (2014). Oncogene ablation-resistant pancreatic cancer cells depend on mitochondrial function. *Nature, 514*(7524), 628-632. doi:10.1038/nature13611

Vonlaufen, A., Joshi, S., Qu, C., Phillips, P. A., Xu, Z., Parker, N. R., . . . Apte, M. V. (2008). Pancreatic stellate cells: partners in crime with pancreatic cancer cells. *Cancer Res, 68*(7), 2085-2093. doi:10.1158/0008-5472.Can-07-2477

Wajid, S., Samad, F. A., Syed, A. S., & Kazi, F. (2021). Ki-67 and Its Relation With Complete Pathological Response in Patients With Breast Cancer. *Cureus, 13*(7), e16788. doi:10.7759/cureus.16788

Wannenmacher, M., Wenz, F., & Debus, J. (Eds.). (2013). *Strahlentherapie* (2., überarb. Aufl. 2013 ed.). Berlin, Heidelberg: Springer.

Westphalen, C. B., Takemoto, Y., Tanaka, T., Macchini, M., Jiang, Z., Renz, B. W., . . . Wang, T. C. (2016). Dclk1 Defines Quiescent Pancreatic Progenitors that Promote Injury-Induced Regeneration and Tumorigenesis. *Cell Stem Cell, 18*(4), 441-455. doi:10.1016/j.stem.2016.03.016

Xia, Y., Jiang, L., & Zhong, T. (2018). The role of HIF-1α in chemo-/radioresistant tumors. *Onco Targets Ther, 11*, 3003-3011. doi:10.2147/ott.S158206

Xu, M., Jung, X., Hines, O. J., Eibl, G., & Chen, Y. (2018). Obesity and Pancreatic Cancer: Overview of Epidemiology and Potential Prevention by Weight Loss. *Pancreas, 47*(2), 158-162. doi:10.1097/mpa.0000000000000974

Xu, Z., Vonlaufen, A., Phillips, P. A., Fiala-Beer, E., Zhang, X., Yang, L., . . . Apte, M. V. (2010). Role of pancreatic stellate cells in pancreatic cancer metastasis. *Am J Pathol, 177*(5), 2585-2596. doi:10.2353/ajpath.2010.090899

Yamaguchi, J., Yokoyama, Y., Kokuryo, T., Ebata, T., & Nagino, M. (2018). Cells of origin of pancreatic neoplasms. *Surg Today, 48*(1), 9-17. doi:10.1007/s00595-017-1501-2

Yao, Y., Xu, X., Yang, L., Zhu, J., Wan, J., Shen, L., . . . Hua, G. (2020). Patient-Derived Organoids Predict Chemoradiation Responses of Locally Advanced Rectal Cancer. *Cell Stem Cell, 26*(1), 17-26.e16. doi:10.1016/j.stem.2019.10.010

ZfKD-RKI. (2016). *Bericht zum Krebsgeschehen in Deutschland 2016*. Berlin: Zentrum für Krebsregisterdaten im Robert Koch-Institut.

Zoa, A., Yang, Y., Huang, W., Yang, J., Wang, J., Wang, H., . . . Tian, Y. (2022). High expression of hypoxia-inducible factor 1-alpha predicts poor prognosis in pancreatic ductal adenocarcinoma: a meta-analysis and database validation protocol. *Transl Cancer Res, 11*(9), 3080-3091. doi:10.21037/tcr-22-787

Publication

Christopher Kessler; Francheska Cadacio; Carlo Maurer, M.D.; Arlett Schäfer; Felix Orben, Ph.D.; Julius C. Fischer, M.D.; Daniela Schilling, Ph.D.; Lisa Fricke; Sebastian Rasch, M.D.; Ihsan E. Demir, M.D.; Katja Steiger, M.D.; Wilko Weichert, M.D.; Roland M. Schmid, M.D.; Stephanie E. Combs, M.D.; Maximilian Reichert, M.D.*; Sophie Dobiasch, M.D.* Establishment of a Translational Radiobiological Platform of Pancreatic Cancer Patient- derived Organoids for Personalized Radiooncology.

Acknowledgements